A genetic toolbox for the turquoise killifish identifies sporadic age-related cancer

Itai Rozenberg[1,5], Roman Franek[1,2, 5], Eitan Moses[1, 5], Tehila Atlan[1], Mathias Diehl[1], Adi Oron-Gottesman[1], Marva Bergman[1], Gwendoline Astre[1], Benyamin Rosental[3], Uri Goshtchevsky[1], Henrik von Chrzanowski[1], Itamar Harel[1,4]

1. Department of Genetics, the Silberman Institute, the Hebrew University of Jerusalem, Givat Ram, Jerusalem, 91904, Israel.
2. University of South Bohemia in Ceske Budejovice, South Bohemian Research Center of Aquaculture and Biodiversity of Hydrocenoses, Zatisi 728/II, 389 25 Vodnany, Czech Republic.
3. The Shraga Segal Department of Microbiology, Immunology, and Genetics, Faculty of Health Sciences, Center for Regenerative Medicine and Stem Cells, Ben Gurion University of the Negev, Beer-Sheva 84105, Israel
4. Corresponding author: itamarh@mail.huji.ac.il
5. These authors contributed equally

Abstract:

Aging is accompanied by a progressive loss of tissue homeostasis, including declining stem-cell function and increased cancer susceptibility. The naturally short-lived African turquoise killifish has emerged as a powerful system for investigating vertebrate aging. However, a critical mass of advanced genetic tools for mechanistic studies has been largely missing. Here, we develop the *Killibow*, a multispectral transgenic line for life-long lineage tracing, an immunocompromised *rag2* mutant for transplantation studies, and genetic mutants for investigating genomic instability and cancer (i.e. *atm* and *tp53*). We performed a series of experiments using this platform, including lineage tracing following germline stem-cell transplantation, and identifying naturally occurring age-related melanoma using engraftment into *rag2* mutants. Exploring tumor dynamics reveals an intriguing age-related interplay between genomic instability and adaptive immunity, accompanied by an evolutionarily conserved decline in immune functions. Together, this toolkit streamlines the investigation of the molecular mechanisms underlying the loss of tissue homeostasis during aging and disease.

Introduction:

As organisms age, they experience an increased susceptibility to diseases and a decline in tissue functions. This is evident through various physiological changes, such as increased cancer incidences and altered stem cell functions[1–6]. At the cellular level, single-cell studies have revealed complex age-related variations in cell composition, cell identity, and lineage commitments within an organ[7–13]. Yet, single-cell transcriptomics methods are constrained by their reliance on discrete temporal snapshots, making them less adaptable to long-term dynamic processes. Therefore, linking molecular identity and cellular lineages in the context of natural aging and related diseases remains experimentally challenging.

With a lifespan of 4-6 months, the turquoise killifish (*N. furzeri*) has recently emerged as an attractive experimental model for studying vertebrate life history at compressed timescales (**Figure 1a**). Notably, the recently established genomic and genome editing resources[14–22] pave the way for developing state-of-the-art genetic tools. In this study, to shed light on the mechanisms that govern tissue homeostasis in health and disease, we develop a comprehensive genetic toolbox for the killifish, which includes lineage tracing and cell transplantation models.

We first introduce the Cre/Lox system to the killifish model and generate the *Killibow*, a transgenic line that allows for stochastic and multispectral lineage tracing. The *Killibow* is based on classical lineage tracing methods previously developed for mice, zebrafish, and medaka[23–31], which have greatly enhanced our understanding of various processes including embryonic development, tissue regeneration, and tumor dynamics[6,32–34]. As a proof-of-principle, we develop germline stem cell transplantation into the killifish testis, an immune-privileged organ. Our findings suggest that each testicular cyst was recolonized by an individual germline stem cell.

To increase the efficiency of transplantation into other organs, we generate an immunocompromised genetic model by mutating the *rag2* gene (recombination activating gene 2)[35–37]. RAG2 is a central component of the multiprotein RAG complex, responsible for generating a diverse repertoire of immunoglobulins and T-cell receptor genes through permutations of V(D)J rearrangements in vertebrates, including killifish[38]. RNA sequencing analysis of *rag2* mutants in the head kidney—a dual-function organ responsible for blood filtering and hematopoiesis in teleosts[39]—highlighted a significant impairment in the

expression of various V(D)J recombination products. Furthermore, using 5' RACE we confirmed that immunoglobulins in *rag2* mutants do not undergo V(D)J recombination.

To utilize our toolbox in the context of aging, we investigated the interplay between DNA damage accumulation and deregulated immune functions in age-related cancer. Specifically, we explored whether sporadic melanocytic expansions previously observed in the tails of old killifish are cancerous, and the possibility that they are be fueled by increased mutational load (e.g. mutating the ataxia telangiectasia mutated gene, *atm*).

Efficient engraftment of sporadic melanoma-like cells into the *rag2* mutants confirmed the occurrence of age-related cancer in killifish. Serial transplantation further increased tumor aggressiveness, allowing successful engraftment also into WT recipients. Yet, paradoxically, when recipients were stratified by age, tumors grew faster in young WT fish compared to old controls, a trend mitigated in *rag2* mutants. This counterintuitive role of adaptive immunity in age-related cancers was previously documented in mice[40], suggesting evolutionary conservation. We further identify functional changes in the immunity of old fish, including a myeloid shift and a decline in phagocytotic capacity.

Our platform is a valuable resource for studying stem cell function, cancer, and tissue regeneration during vertebrate aging, and it complements existing models by shortening experimental timescales.

Results

Generation of an inducible *Killibow* transgenic line

To generate the *Killibow* transgenic line we used the *Zebrabow* construct[23]. The default expression of this construct is dTomato, a red fluorescent protein (RFP). Following Cre-mediated recombination, the expressed reporter is switched to either mCerulean, a cyan fluorescent protein (CFP), or EYFP, an enhanced yellow fluorescent protein (YFP, **Figure 2a**, left).

This discrete expression, of either RFP, CFP, or YFP, is made possible by two pairs of Lox sites, LoxP and Lox2272, which are mutually incompatible. Thus, recombination is irreversible and can occur only once. Reporter expression is controlled by the zebrafish ubiquitin promoter[41], which is robustly expressed in various vertebrate models, including killifish[42–44]. We have recently confirmed its activity in multiple killifish organs using FACS[45], such as the muscle, brain, liver, heart, skin, and gut.

Tol2-based transgenesis was performed in fertilized killifish eggs[15,20], and a founder transgenic line with bright RFP expression was selected. Using standard qPCR approaches[46,47] we estimated that the number of transgenic insertions in the *Killibow* line is ~24 (see **Methods**). In the absence of Cre recombination, *Killibow* fish exclusively expressed RFP (**Figure 2a**, right). Similar to what is observed in zebrafish[23], expression was initiated during early somitogenesis (**Figure S2a**) and persisted to adulthood (**Figure 2a**, right).

Heritable multicolor stochastic labeling mediated by Cre recombination

To test Cre-mediated recombination, we first generated a primary fibroblast culture derived from the tail of a naïve *Killibow* fish. To develop a stable cell line, we co-transfected these cells with a Tol2-Doxycycline-inducible *Cre* plasmid and a Tol2 transposase-encoding plasmid. Cells were selected for plasmid integration using puromycin selection (see **Methods)**. This cell line was treated with Doxycycline, displaying highly diverse multicolor labeling (**Figure 2b**, left).

To test recombination in live fish we microinjected *Cre* mRNA into one- or two-cell stage *Killibow* embryos. Injected fish displayed colorful labeling, which appeared during early somitogenesis and persisted to adulthood (**Figure 2b**). High *Cre* mRNA concentrations (~20 ng/µl, in ~10 pl of injection mixture) produced fish that expressed only a blue/green color combination, probably due to saturation of recombination (**Figure S2b**).

At lower mRNA concentrations (~5 ng/µl) we obtained multicolor labeling throughout the killifish body (**Figures 2b, S2c**). The relatively large clones observed in several internal organs are most likely due to recombination occurring in early development. Within organs, dorsal muscle sections revealed color boundaries between fiber clusters, suggesting distinct embryonic origins (**Figure 2b**, right).

We then crossed *Cre*-injected adult *Killibow* fish with WT fish. Offspring were uniformly colored in a single hue (**Figure S2d**), indicating stable labeling of the germline. To induce Cre-mediated recombination in adult tissues, we utilized our recently developed *in-vivo* approach[19] (**Figure S2e**, top) to electroporate a *Cre-gfp* plasmid following intramuscular injection. As it is difficult to distinguish between plasmid-encoded GFP and the YFP in the *Killibow* construct, only the emergence of CFP was used to assess successful recombination (**Figure S2e**, bottom). Finally, tail-fin amputation[48] further suggested that color combinations are stable during regeneration, as hues were comparable between the original and newly-

formed tissue (young or old fish, n=3 for each group, **Figure S2f-g**). Our results demonstrate that Cre-mediated recombination produces stochastic and stable labeling in killifish.

Germline stem cell transplantation from *Killibow* to WT fish

We then designed a proof-of-principle experiment to track cell lineages following spermatogonial stem cell transplantation. To this end we adapted a protocol developed for zebrafish[49], taking advantage of the testis as an immune-privileged organ[50] (**Figure 2c**). Briefly, depletion of endogenous spermatogenesis in male killifish recipients was performed using gradual heat treatments followed by a busulfan injection. Germline ablation was confirmed 12 days post-injection by the absence of the germline marker DDX4 (n=5, **Figure 2c**, center).

Next, a single-cell suspension of *Killibow* testicular cells was transplanted into germline-ablated recipients through the genital pores. Four weeks following transplantation the testis was removed and imaged. As in many vertebrate males, killifish germline cells develop within a cyst—the basic functional unit of the testis[51]. While multicolor colonization of the testes was confirmed, our data suggested that for each cyst, transplantation was probably mediated through an independent unicolor clone (**Figures 2c**, right, and **S2h**).

Analyzing the color profile of images of *Killibow* cells, embryos, and muscle fibers suggested high diversity, consistent with the predicted number of copies of the *Killibow* cassette in the killifish genome (**Figure 2d**). However, as diversity was reduced in the transplanted testis, we hypothesize that this is probably a result of the limited number of founder stem cells (**Figure S2h**). Our proof-of-principle experiment shows that the *Killibow* transgenic model can be effectively used for lineage tracing in both naïve and manipulated fish.

Generation and characterization of a *rag2* genetic model

To enable transplantation into other organs, aside from the testis, we generated an immunocompromised genetic model by mutating the *rag2* gene[35–37] (**Figure 3**). Using our recently updated CRISPR protocol[20,52] we generated a ~250 base-pair deletion allele (Δ250) in the single exon of the killifish *rag2* coding sequence (**Figure 3a**, left). We outcrossed this line for several generations and generated a fertile homozygous fish.

Murine *rag2* mutants display hematopoietic and immune system defects, including arrested B-cell and T-cell development[53]. Therefore, we compared the transcriptome of the killifish head kidney from three male WT and three male *rag2* mutants. Principal component analysis (PCA) demonstrated that both groups segregate according to PC3 (**Figures 3a**, **S3a**).

The differential expression analysis revealed 14 downregulated and 3 upregulated genes (fold change > 2, FDR <0.05, **Figures 3b**, **Table S1**). Interestingly, downregulated genes were directly related to *rag2* functions, including members of the immunoglobulin gene family (**Figure S3b**). These data suggest that failure to rearrange the V(D)J gene segments perturbs expression.

Upregulated genes were sparse, and linked to immune and signaling-related pathways, including the novel immune-type receptors (NITRs)[54–59], (i.e. *nitr13.2*, **Figure S3b**). NITRs have been identified in all major lineages of teleost fish[60], and are structurally similar to the killer immunoglobulin-like receptors (KIR) on mammalian natural killer (NK) cells[58]. These receptors do not depend on V(D)J recombination[60] and are expressed in teleost NK-like cells[58,61]. Interestingly, an expansion of NK-like cells was previously detected in zebrafish *rag2* mutants[57], suggesting an evolutionary conserved mechanism.

Lack of V(D)J recombination in *rag2* mutants

The killifish immunoglobulin heavy chain (*igh*) gene locus[62] consists of a constant region (C), and several variable V(D)J regions (**Figure 3c**, top). To assess V(D)J recombination in *rag2* mutants we adapted a recently developed 5' RACE protocol[38]. Briefly, we extracted RNA from the head kidneys of WT and *rag2* mutant fish and performed cDNA amplification using a specific primer for the constant region. Template-switching further allowed us to amplify all *igh* recombination variants (**Figure 3c**, center, and see **Methods**).

This protocol produced a ~600 base pair amplicon in WT fish, consistent with mature immunoglobulins[38]. Conversely, we did not detect these amplicons in *rag2* mutants (**Figure 3c**, bottom), and shorter faint bands are likely a result of non-specific amplification. This suggests the absence (or significant reduction) of V(D)J recombination in *rag2* mutants. Next, we performed a series of experiments to utilize the developed toolkit as a valuable resource for functional aging studies.

Identification and characterization of sporadic age-related melanoma in killifish

So far, the presence of age-related cancer in killifish has been a topic of debate. While early studies reported a high incidence of age-dependent liver neoplasms[63], more recent findings have linked proliferative lesions in internal organs to a host-defense response against mycobacterial infections[64]. Similarly, pre-cancerous changes in the intestine were previously detected only in telomerase-deficient killifish[14]. While sporadic age-related expansion of tail

melanocytes has been cautiously referred to as "tissue homeostasis defects"[65], further investigation was required to confirm their cancer-like characteristics.

Tumor transplantation studies into an immunodeficient host are a vital approach for investigating cancer biology in model organisms[37,66,67]. As the first step in developing intramuscular transplantations, we used *Killibow*-derived cells to facilitate visual confirmation of successful injections (**Figures S4a, b**, see **Methods**). As expected from non-malignant cells, while the injected cells were initially detected in *rag2* mutants, they did not persist (n=10, **Figure S4b**).

In contrast, cells isolated from a melanocyte expansion in the tail of an old fish were successfully engrafted and generated an extensive melanoma-like tumor, specifically in *rag2* mutants (**Figure 4a**). As a control, these cells failed to engraft when transplanted into WT fish (0/3). Similarly, phenotypically normal melanocytes isolated from the tail of a young fish did not engraft into *rag2* mutants (0/3).

Following successful engraftment (**Figure 4a**), melanocytes were detected in multiple organs, invading skeletal muscle, blood vessels, connective tissue, and the kidneys (**Figure 4b**). To visualize cell proliferation, tumor cells were engrafted into a new *rag2* recipient, and six weeks following engraftment the fish were injected with EdU (5-Ethynyl-2'-deoxyuridine, see **Methods**). Following an H_2O_2 treatment to remove the dark melanin, which can obscure the fluorescence signal, many EdU-positive nuclei were detected within the melanocyte-positive area (**Figure 4c**).

Exploring mutation accumulation and immune function in age-related cancer formation

The formation of tumors depends on the accumulation of mutations on one hand, and the ability of the immune system to clear pre-cancerous cells on the other. To first accelerate mutation accumulation, we generated loss-of-function models for *tp53* (**Figure S5a**) and *atm* (**Figure 5a**, left). *tp53* is a well-established tumor suppressor[68–70], and in agreement with previous findings, primary cells isolated from $tp53^{\Delta 14/\Delta 14}$ mutants displayed hyperproliferation and a modified response to DNA-damage-induced apoptosis (**Figure S5b**). The *atm* gene is a master regulator of genome stability and the DNA damage response (DDR). Accordingly, old *atm* mutant fish display an increased incidence of melanoma-like splotches in the tail (5/5) compared to age-matched WT controls (0/9, Fisher's exact test = 0.0005, **Figure 5a**, right). These data suggest that increasing mutational load might contribute to age-related cancer in killifish.

Next, to explore the relative interplay between age and adaptive immune functions during cancer engraftment, we performed transplantations into WT and *rag2* mutant fish, young or old, using serial transplantations (**Figure 5b**, left). Following transplantation into WT (n=12) and *rag2* mutants (n=8), 25% of the WT fish died within a week, while no mortality (0/8) was observed for *rag2* mutants (**Table S2**). As suggested in the zebrafish *rag1* mutants, the enhanced survival in the first few days following injection could be related to compensatory innate immunity (e.g. expansion of NK cells[71,72]).

We then evaluated tumor engraftment 5-6 weeks post-injection. From the surviving fish, 100% of the *rag2* mutants exhibited tumor-like melanocyte expansions around the injection site. Conversely, only ~50% of WT fish showed any sign of a tumor (Fisher's exact test =0.03, **Figure 5b, Table S2**), suggesting that *rag2* is a better recipient. The successful engraftment in WT fish could be attributed to serial tumor transplantations, which are known to increase tumor aggressiveness[73,74]. Accordingly, in the 3rd passage and onwards, successful engraftment was detected in all recipients, regardless of genotype (WT recipients, n=15/15 for passage 3, and n=18/18 for passage 4).

To evaluate tumor size, we visually classified the area of pigmented tumors. Stratifying the recipients by age revealed a reverse trend between WT and *rag2* mutants. Specifically, while in WT fish, medium to large tumors were more prevalent in young individuals, tumor size correlated with age in *rag2* mutants (Fisher's exact test =0.006, comparing the four experimental combinations of age and tumor size between WT and *rag2* mutants, **Figure 5b, Table S2**).

Interestingly, similar trends were recently observed in mice[40], demonstrating that although cancer incidence increases with age, successfully engrafted cancers grow faster in a young niche. As this pattern was similarly abrogated in *rag1*^{null} mice, age-related cancer progression probably depends on an evolutionary-conserved role of adaptive immunity[40]. Yet, the changes in the killifish immune system during aging have only recently started to be explored[38].

Age-related functional decline in the killifish immune system

During human aging, the immune system undergoes several classical changes. For example, hematopoietic stem cells exhibit an increased tendency to differentiate towards myeloid lineages[75–77] (which are associated with innate immunity). This phenomenon is referred to as

"myeloid shift", and is accompanied by a diminished ability to differentiate into lymphoid/adaptive lineages.

To explore overall lineage composition in killifish immunity we employed flow cytometry on peripheral blood and the head kidney (as previously developed for zebrafish[78,79]). Using forward scatter (FSC, which corresponds to cell size), and side scatter (SSC, which relates to cellular granularity), we were able to isolate the primary hematopoietic lineages: erythroid cells (FSC^{low}), myeloid lineages ($FSC^{high}SSC^{high}$) and lymphoid cells ($FSC^{mid}SSC^{low}$) in both the head kidney and peripheral blood (**Figure 5c**, left). Sorting cells from each population followed by GIEMSA staining further confirmed that cellular morphology is highly conserved with zebrafish[78], and consistent with their mammalian counterparts, albeit with some distinctions (e.g. mammals lack nucleated erythrocytes).

Next, to investigate the existence of a "myeloid shift" in aging killifish, we expanded our flow cytometry analysis to include old and young fish (n = 6 for each group). We show that the ratio between myeloid and lymphoid lineages significantly increased by ~ 2-fold with age, indicating that an age-related myeloid shift is evolutionarily conserved ($p = 0.0004$, **Figure 5c**, center).

To further examine immune functions, particularly phagocytosis, we incubated immune cells with fluorescent beads (green) and co-stained them with a lysosome dye (red). Using flow cytometry, we demonstrate that despite the increased abundance of myeloid cells with age, their functional quality is compromised. We further confirmed the intracellular localization of the beads using a confocal 3D reconstruction (**Figure 5c**, right). These findings indicate that classical age-related features of the systemic milieu in humans[75–77] are conserved in killifish immunity.

In conclusion, our comprehensive set of tools combines multispectral lineage tracing, a transplantation model, and DDR loss-of-function mutations, together facilitate the exploration of key aspects of tissue homeostasis, particularly stem cells and cancer.

Discussion:

As the most diverse group of vertebrates, fish species exhibit a vast range of evolutionary adaptations, providing an experimental playground for modeling complex traits in health and disease[80–84]. Here, we describe the development of a genetic toolkit for the naturally short-lived turquoise killifish, which can be used to explore various aspects of tissue homeostasis, including stem cell function and cancer biology.

The strength of the multicolor *in vivo* labeling is particularly demonstrated through germline stem cell transplantation. Expanding this strategy in the context of aging, such as by studying the ability of young and old spermatogonial stem cells to colonize the gonad, or monitoring the borders between different clones within an organ, could indicate progressive changes in tissue homeostasis. Similarly, lineage composition can allow us to discriminate between alternative mechanisms of cellular senescence. Specifically, whether they are more likely to originate from a limited number of damaged stem cells, in which case we would detect that senescent cells display a lower color complexity when compared to the surrounding tissue. Alternatively, if this is a random event, senescent cells will have a comparable hue distribution to the surrounding tissue.

Introducing the Cre/Lox system to the killifish model should stimulate the killifish community to further generate tissue-specific and inducible *Cre* drivers. Yet, it is worth mentioning several limitations of the *Killibow* line, including the transgene positional effect, and loss of color diversity due to the reduction of copy numbers that segregate over time. To mitigate these challenges, the *Killibow* line could be propagated by intercrossing (and selecting only bright-red individuals) and preserved using sperm cryopreservation[85].

The *rag2* immunodeficient model facilitated the identification of melanoma-like cancer, which sporadically occurs during killifish aging. Similar to the role of stem cells in normal tissue homeostasis, tumor growth can also be modified by cancer stem cells[6,32,33]. While lineage-tracing techniques have provided insights into tumor dynamics (e.g. the therapeutic response of cancer stem cells[86]), how lineage composition is modified in tumors by the aging microenvironment remains largely unknown[6].

The killifish immune system[38,87] is largely underexplored when compared to other, relatively well-studied hallmarks of aging in killifish, including deregulated nutrient sensing[88,89], telomere atrrition[14,15], and loss of protein homeostasis[45,90,91]. By exploring the contribution of mutation accumulation and immune functions to age-related cancer, we demonstrate that these aging hallmarks can promote cancer incidences. However, it should be noted that *atm*-deficient patients (suffering from the A-T syndrome[92–94]) also display a compromised immune system. Therefore, as the interplay between immunodeficiency, mutation accumulation and cancer predisposition is complex[95], we cannot rule out the contribution of a dysregulated immune system to the increase in cancer incidence in this model.

Our engraftment studies highlight a seemingly paradoxical trend. Specifically, while young WT fish are more resistant to tumor engraftment, successful engraftment produces larger tumors. The reversal of this trend in the immunocompromised *rag2* mutants proposes an important role in adaptive immunity. Indeed, similar results in mice identify that age-related tumor growth is related to integrin α 4 (*itga4*) in $CD8^+$ T cells[40], suggesting that the interplay between the immune system and age-related cancer progression is evolutionarily conserved. These data demonstrate the usefulness of the killifish for the study of the aging tumor microenvironment.

Together, we add to the expanding tools available for the killifish model system[52,96–98], by providing a useful resource for investigating cell dynamics during vertebrate aging and disease.

Figure legends:

Figure 1: Generation of the *Killibow* transgenic line

a) The life history of the African turquoise killifish (*N. furzeri*), including development, puberty, and aging. Fish reach sexual maturity after 2-3 weeks post-hatching and display typical signs of vertebrate aging after a few months. dpf, days post-fertilization; dph, days post hatching; mph, months post-hatching.

Figure 1

a. The turquoise killifish, a naturally short-lived vertebrate with a compressed lifespan

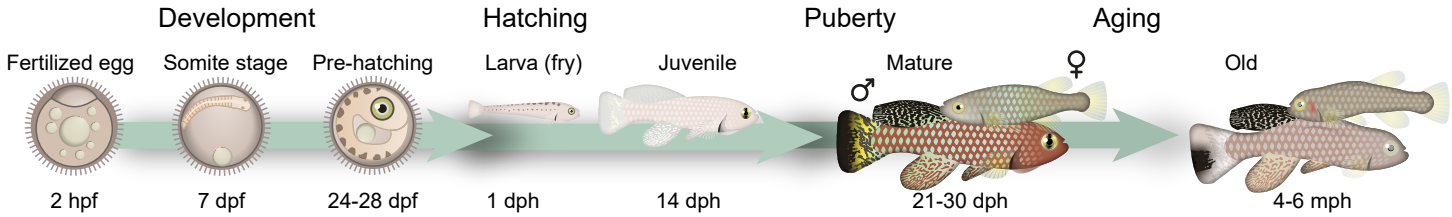

Figure 2: Lineage tracing following germline stem cell transplantation

a) The *Zebrabow* construct[23] (left) was used to generate the *Killibow* transgenic line (right). The Cre recombinase can recognize either Lox2272 (purple arrowheads) or LoxP (orange arrowheads) sites, resulting in the excision of sequences flanked by the Lox sites. Because Lox2272 and LoxP are mutually incompatible, recombination occurs only between identical Lox sites (event 1 or 2, bottom left).

b) Stochastic multicolor labeling is visible in *Killibow*-derived cells expressing a Doxycycline-inducible *Cre* (left), in embryos injected with *Cre* mRNA (center), and in the tail and muscle sections of *cre*-injected adult fish (right). Images are representative of n≥6.

c) Development of germline stem-cell transplantation in killifish. Germline depletion in WT recipients was performed through heat and busulfan treatments (left). Depletion efficiency was confirmed by staining histological sections using a germline marker (DDX4, magenta). Successful engraftment following transplantation of *Killibow*-derived germline stem cells (right). n ≥ 4 biological replicates for each experimental condition.

d) Hue/saturation plots of the different colors shown in panels (**b**) & (**c**), including cells, embryo, muscle fibers, and testis transplanted with *Killibow*-derived germline stem cells.

Figure S2: single clones repopulate spermatogenic cysts

a) Fluorescent expression in the *Killibow* transgenic line is first visible during somitogenesis (st. 30[99]). Image representative of n≥6 for each stage.

b) A high concentration of *Cre* mRNA saturates recombination to the point that the red color is no longer visible. Image representative of n=6.

c) Dissection of selected organs in *Cre*-injected fish demonstrates widespread multi-color labeling. Image representative of n=6.

d) Mating *Cre*-injected fish with WT fish produces a variety of single-colored offspring, demonstrating unicolor germline transmission. Images representative of offspring from n = 4 couples.

e) Schematic illustration of the intramuscular plasmid electroporation approach (top). Because GFP cannot be easily distinguished from transgenic YFP, only CFP is used to validate successful recombination (bottom, n = 4).

f) Experimental workflow for assessing tail-fin regeneration (left). Following amputation, regrowth was measured every three days for a total of 18 days. The white dashed line represents the amputation plane, and an enlarged view shows an example of partial tail fin regeneration (right).

g) Examples of regenerated tails at day 18 post amputation, in young (left) or old (right) *Cre*-injected *Killibow* males. Green autofluorescence from regenerating bones is marked by an asterisk. n ≥ 4 biological replicates for each experimental condition.

h) Tissue sections following germline stem-cell transplantation in the testis. A uniform color in each cyst (white asterisk) suggests that they were repopulated by individual clones. Image representative of n=4/10 successful transplantations.

Figure 2

a. Generation of the *Killibow* transgenic line

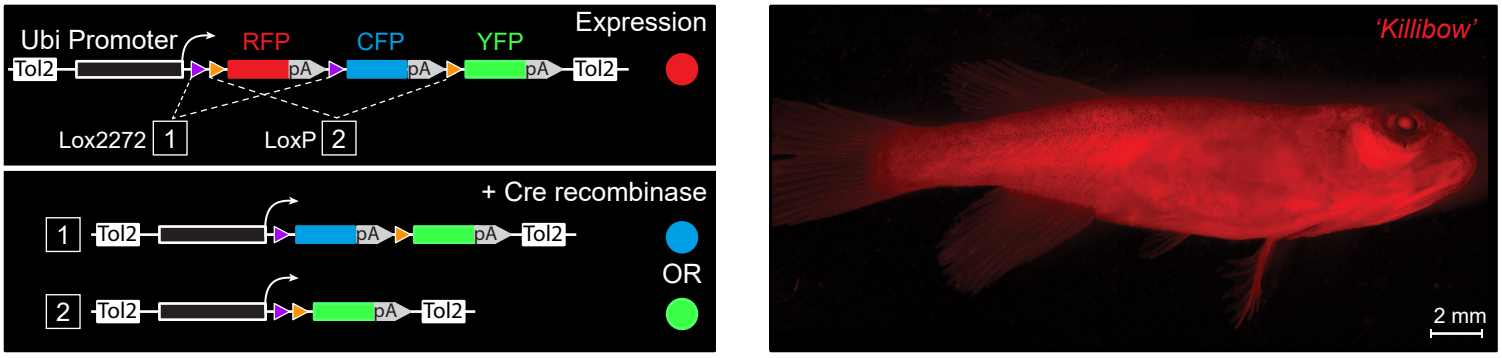

b. Stochastic multicolor labeling following *Cre* mRNA injection

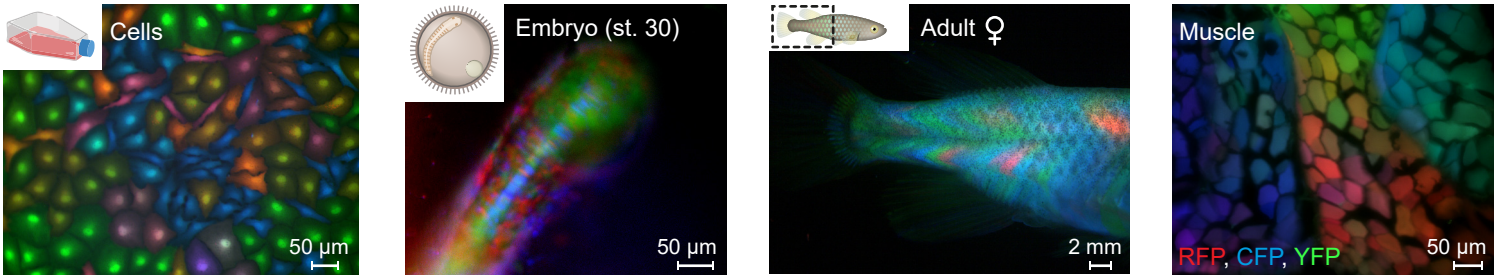

c. *Killibow* testicular stem cell transplantation

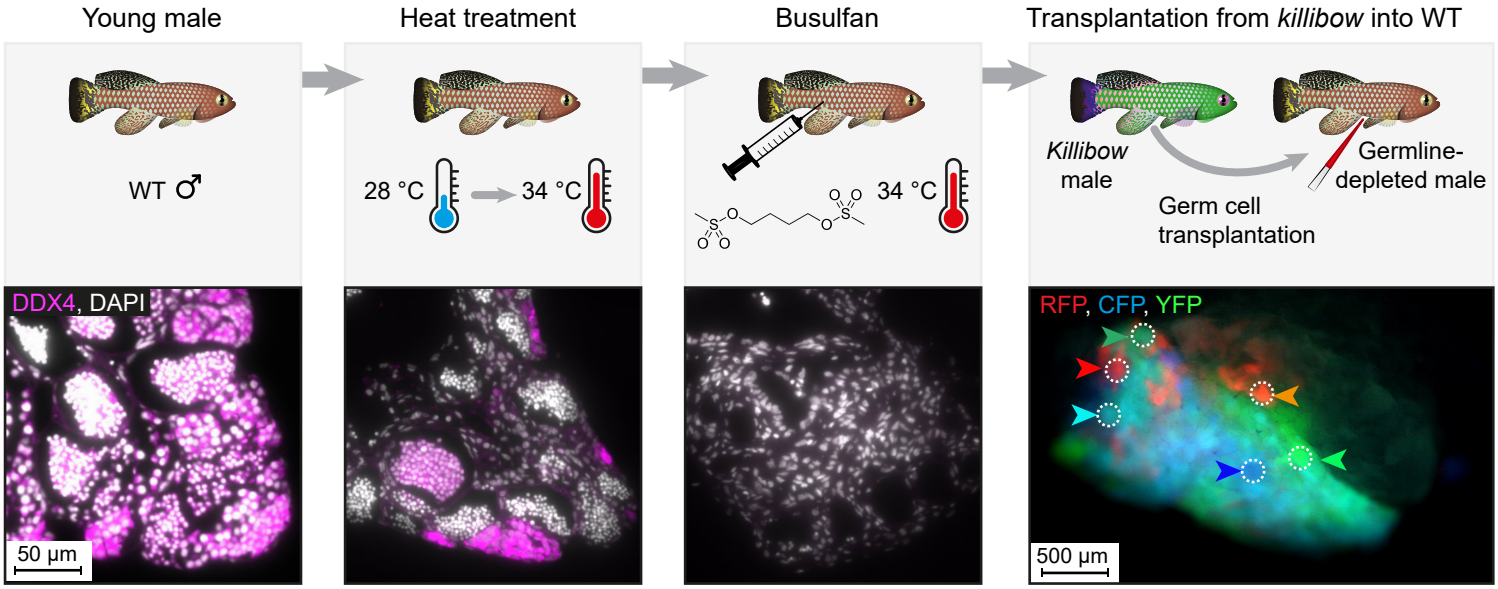

d. Assessing color profiles

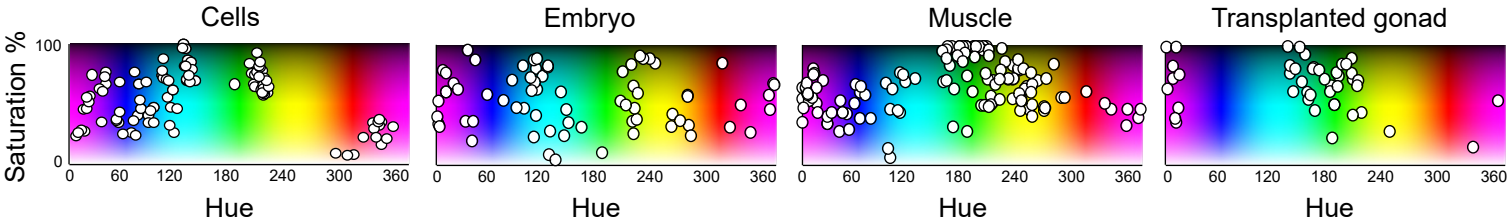

Figure S2

a. *Killibow* expression in early embryonic development

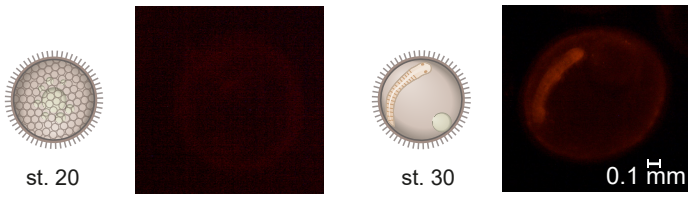

b. Saturated *Cre*-mediated recombination

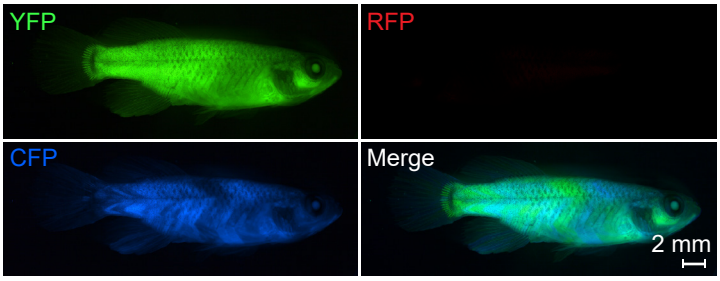

c. Labeling of internal organs

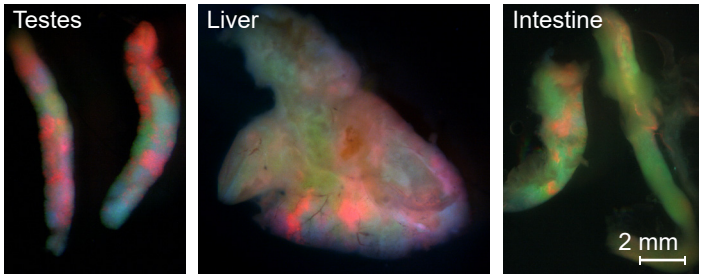

d. Unicolor germline transmission following *Cre* mRNA injection

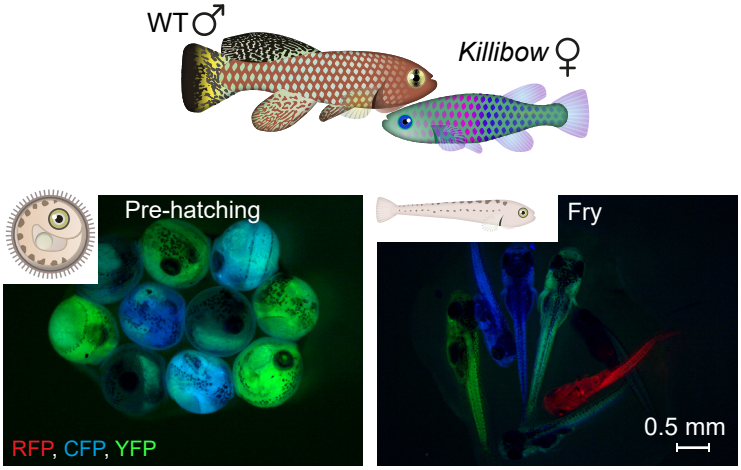

e. A plasmid electroporation system for inducible *Cre*-mediated recombination

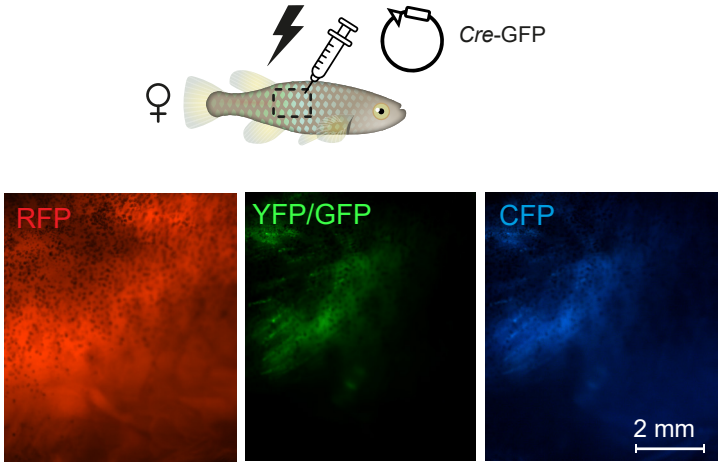

f. Exploring organ-level tissue regeneration

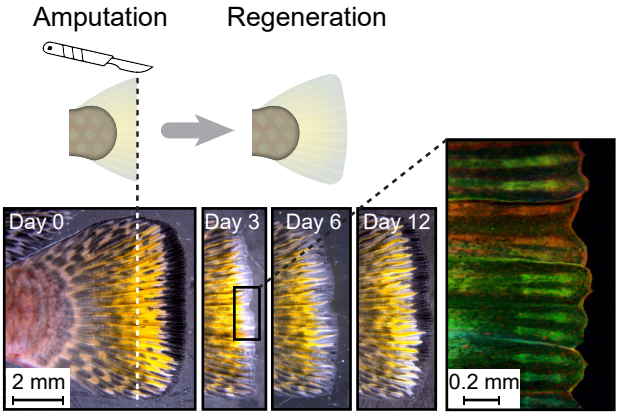

g. Regeneration dynamics through aging

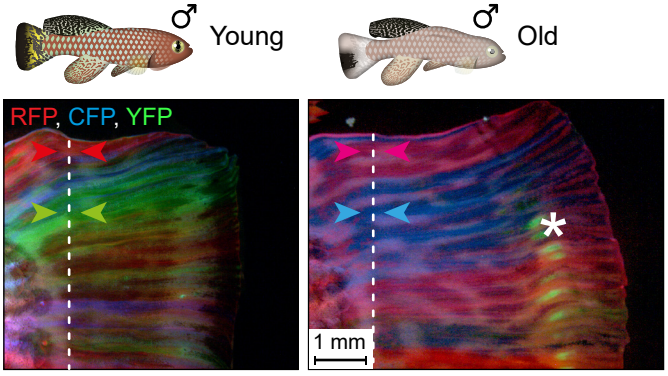

h. Gonadal section following testicular stem cell transplantation

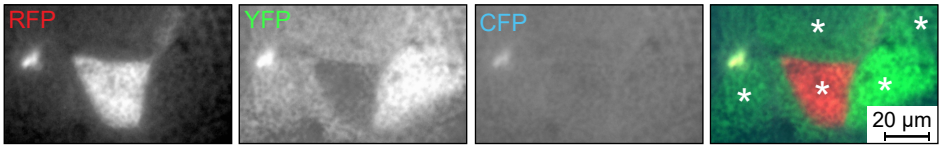

Figure 3: Generation of an immunodeficient killifish model

a) Generation of a *rag2* CRISPR mutant with a ~250 bp deletion (Δ250). A gene model with a single exon is shown (left). Following RNA sequencing for the head kidney of WT (black) and *rag2* mutant fish (green), principal component analysis (PC1/PC3) is shown. Each symbol represents an individual fish (right).

b) Volcano plot presenting the differential gene expression between WT and *rag2* mutant fish. The dashed lines represent the statistical thresholds for the GO analysis (fold-change = 2, FDR = 0.05). Upregulated genes are in red, and downregulated genes are in blue.

c) A schematic model of the killifish *igh* genomic locus, including the constant region (C) and variable regions (top). Experimental design of the V(D)J recombination assay, including RNA isolation, region-specific reverse transcription, and PCR amplification (center, adapted from[38,62]). Agarose gel of the PCR amplified *igh* locus from WT and *rag2* mutant fish, n=3 for each genotype (bottom). Non-specific amplification is marked by an asterisk.

Figure S3: Altered immunity in *rag2* mutant fish

a) PC1/PC2 for transcript levels from the head kidney of WT (black) and *rag2* mutant fish (green). Each symbol represents an individual fish.

b) Bar-plot of selected upregulated (left) and downregulated (right) genes, normalized to the WT. Error bars represent mean ± SEM. Significance was called as part of the edgeR pipeline. FDR-corrected p-values are indicated.

Figure 3

a. Generating an immunocompromised killifish model by mutating *rag2*

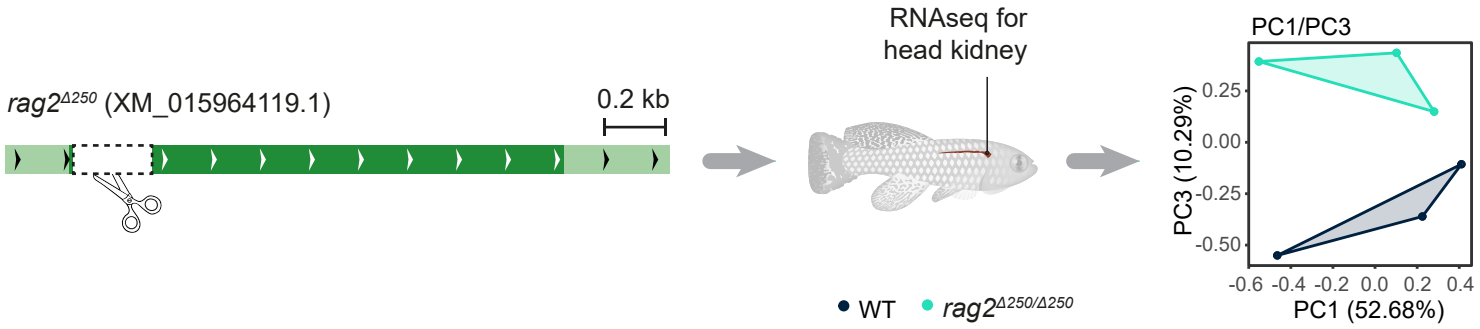

b. Volcano plot highlights the involvement of adaptive and innate immunity

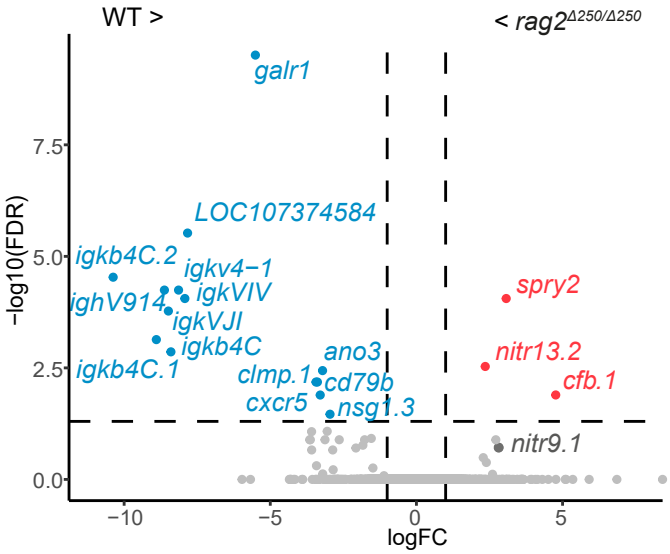

c. Assessing V(D)J recombination in *rag2* mutants

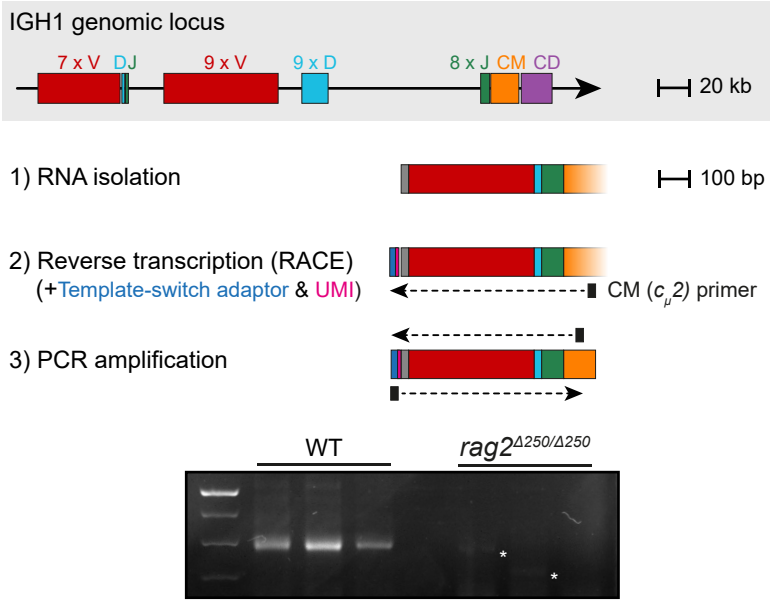

Figure S3

a. PCA for transcript levels in the head kidney

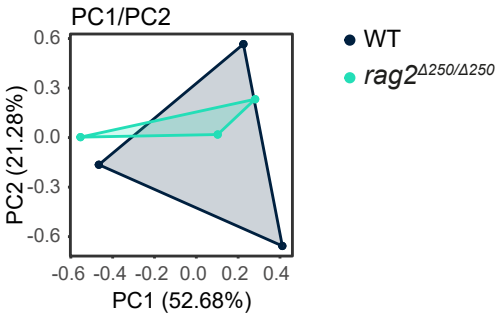

b. Barplot of selected up-regulated genes

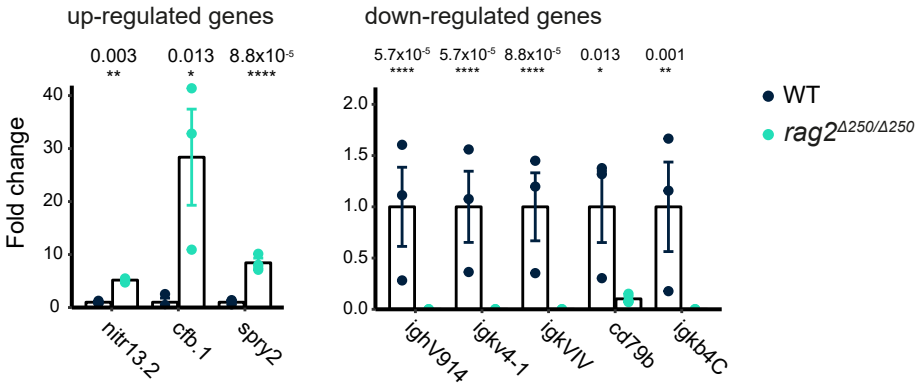

Figure 4: Identification of an age-related melanoma in killifish

a) Engraftment of primary cells derived from a melanocyte expansion in the tail of a 7-month-old fish into *rag2* mutant recipients results in a melanoma-like tumor. n = 3 biological replicates. Scale: 5mm

b) H&E staining for the fish seen in (**a**) highlighting multi-organ invasion.

c) Experimental design (left). Detecting cell proliferation by EdU staining (center), in a histological section from the fish engrafted with melanoma cells in (**a**). The slide was treated with H_2O_2 to remove the melanin pigment. Bright field image of an adjacent section not treated with H_2O_2, in which melanocytes are visible (right). The dashed line marks the corresponding area. Representative of n = 3 individuals. Scale: 50µm

Figure S4: Transplantation of *Killibow*-derived fibroblast cell line

a) Injection of *Killibow*-derived cells into WT fish. n = 10 biological replicates.

Figure 4

a. Engraftment into *rag2*$^{\Delta 250}$ mutant fish

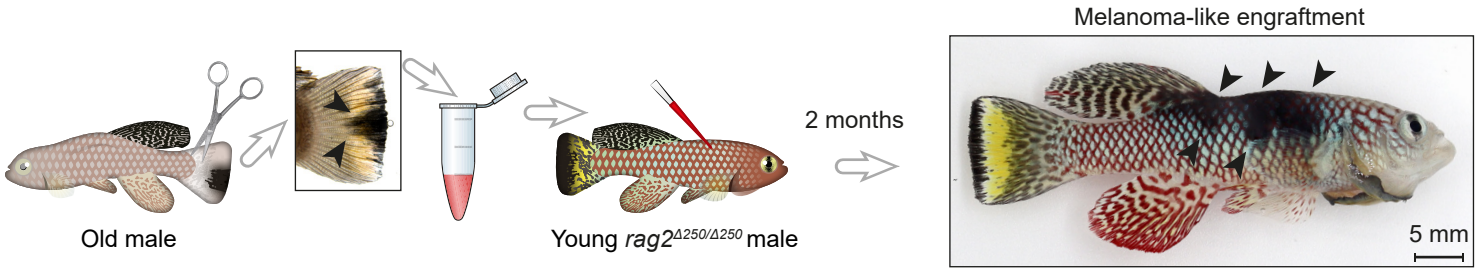

b. Multi-organ invasion following engraftment of into *rag2*$^{\Delta 250}$ mutant fish

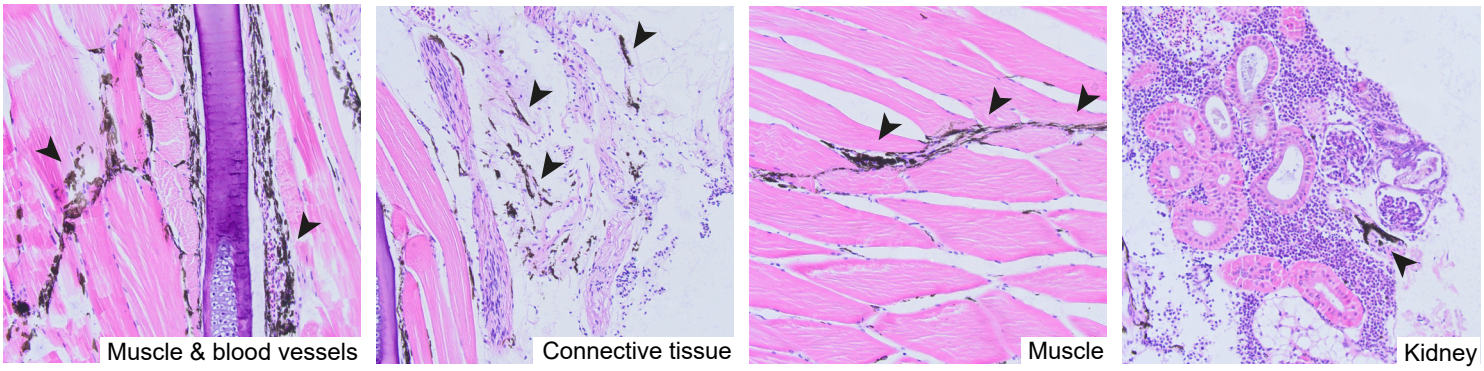

c. EdU proliferation assay in the muscle of engrafted fish

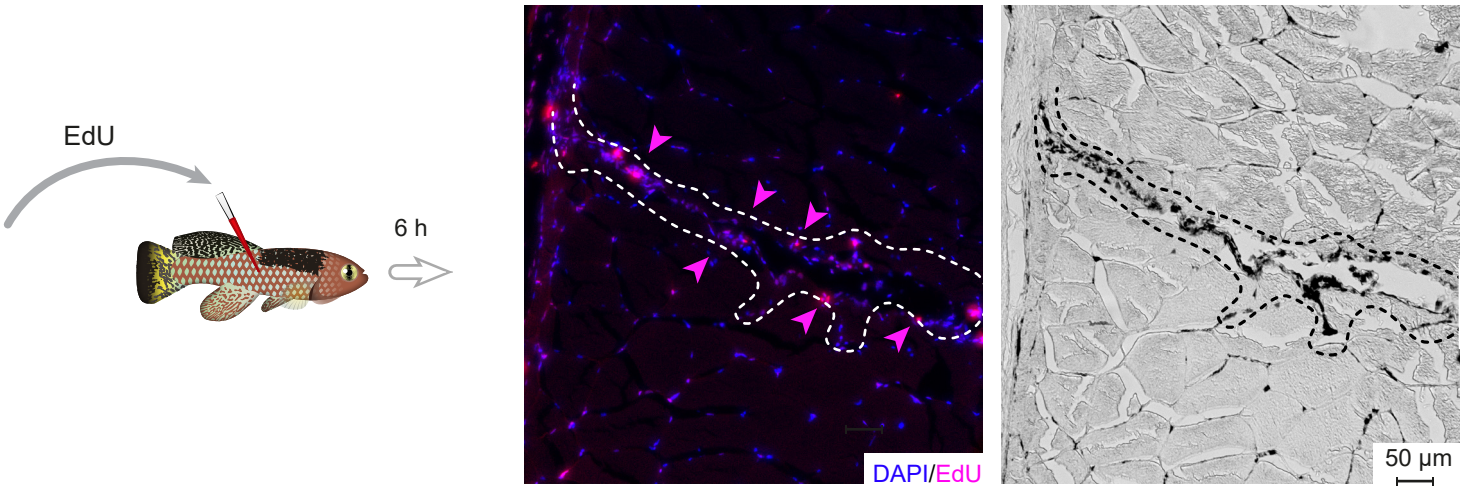

Figure S4

a. Transplantation into *rag2*$^{\Delta 250}$ mutant fish

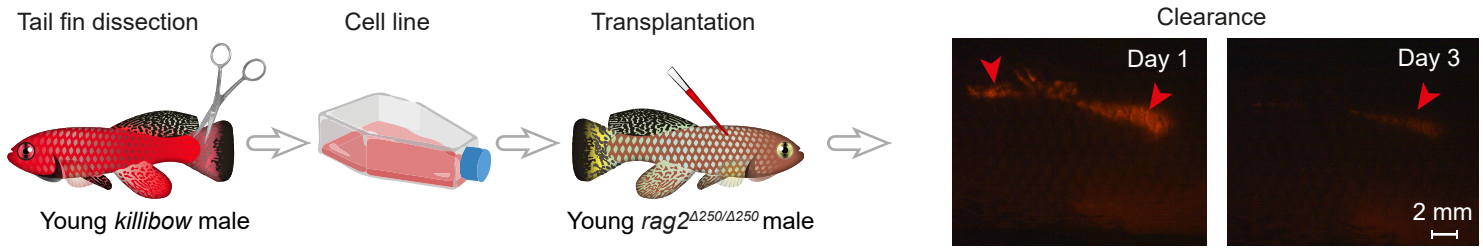

Figure 5: Age-related cancer is modified by mutation accumulation and altered immunity

a) Generation of an *atm* CRISPR mutant with a 4bp deletion (Δ4). A gene model with exons is shown, with the mutation site marked with a red asterisk, the gRNA target in red, and the protospacer adjacent motif (PAM) in bold. Representative images of ~10-month-old WT and $atm^{\Delta 4/\Delta 4}$ mutant fish depicting melanocyte expansion in the tail (black arrow). Experimental group sizes are indicated.

b) Representative images of WT and *rag2* mutant fish injected with a melanoma cell suspension. The black arrow and dashed line indicate the injection site and visible tumor boundaries. For a full analysis of tumor progression see **Table S2**.

c) Left: kidney marrow and blood cells analyzed by flow cytometry, using forward scatter (FSC) and side scatter (SSC) to separate populations of red blood cells, lymphocytes, and myeloid cells. Center: GIEMSA stains of sorted cells from the indicated gates. Left bar graph: analysis of the shift from lymphocytes toward myeloid lineages in older fish. Right bar graph: following incubation with green fluorescent beads, cells were analyzed by flow cytometry for phagocytosis by myeloid cells. Error bars indicate mean ± SEM. n=6 individuals for each experimental condition. Significance between young and old fish was calculated using a two-sided Student's t-test with the indicated p-values. Right: confocal analysis of cells after phagocytosis of fluorescent beads (green). Cells were co-labeled with either a red lysosome dye (LysoTracker; top) or a non-specific membrane dye (DiI) and visualized with a 3D surface analysis to show the internalization of the beads (bottom). Scale bar = 5 µm.

Figure S5: *tp53* mutation causes hyperproliferation in cells

a) Generation of a *tp53* CRISPR mutant with a 14 bp deletion (Δ14). A gene model with exons is shown, with the mutation site marked with a red asterisk, gRNA targets in red and PAM in bold.

b) Characterization of $tp53^{\Delta 14/\Delta 14}$-derived cells. Proliferative capacity (left) was measured on days 1 and 5. Significance was calculated using a two-way ANOVA with Sidak`s post-hoc, n=9 replicates. Survival (right, normalized to WT) was assessed four days following etoposide treatment. Significance was calculated using an unpaired, two-sided t-test. P-values are indicated, n=9 replicates.

Figure 5

a. DDR mutants for *atm* display increased melanoma incidence in very old fish

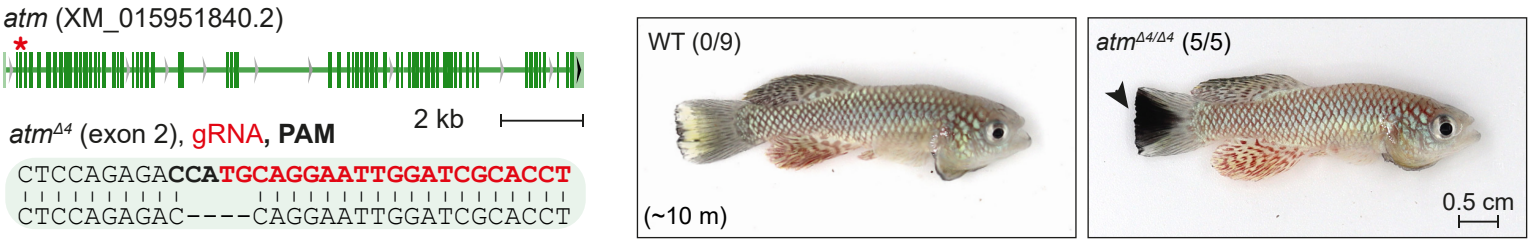

b. Age-related increase in early-stage engraftment in *rag2* mutants

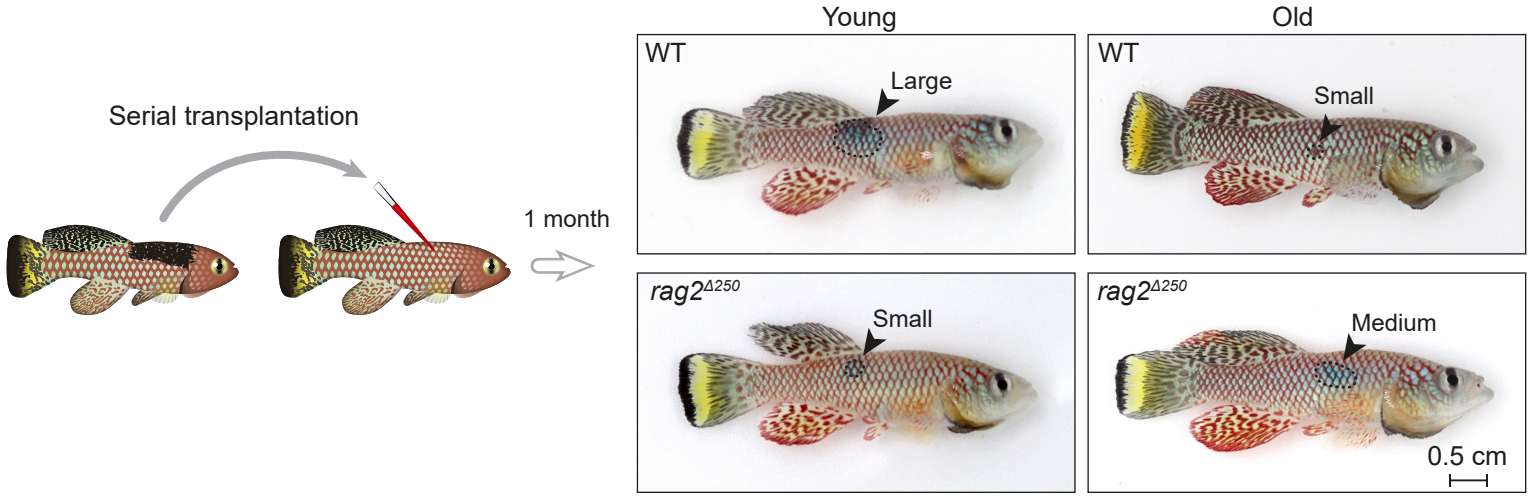

c. Age-related changes in immune cell function and composition

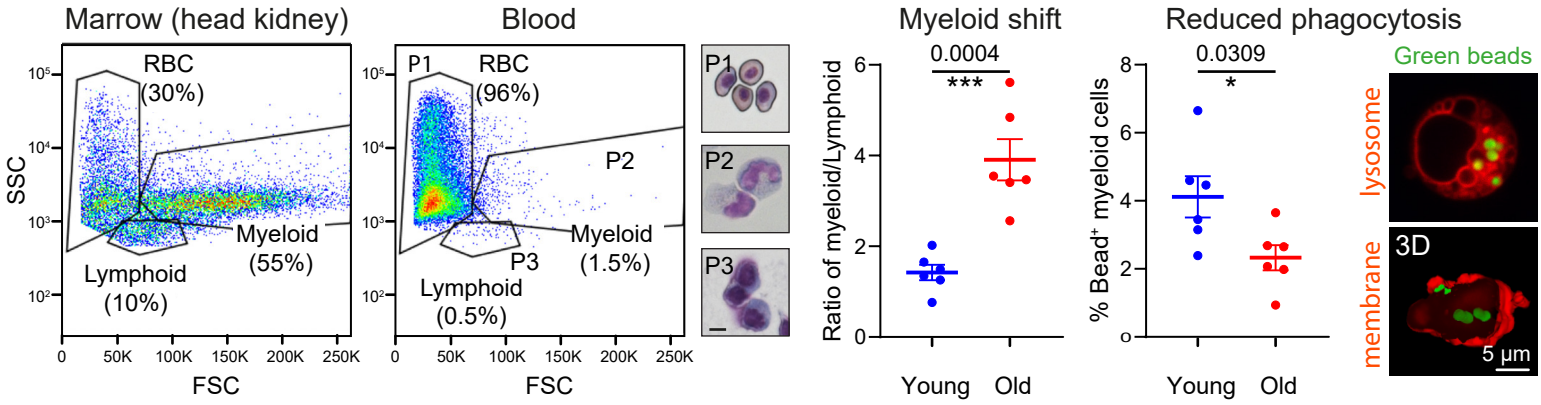

Figure S5

a. Generating a *tp53* mutant

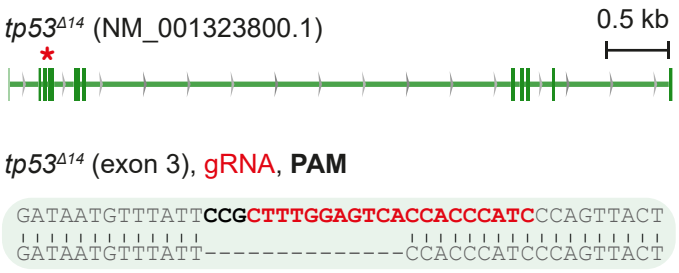

b. *tp53*$^{\Delta14/\Delta14}$-derived cells display modified proliferation and response to DNA-damage

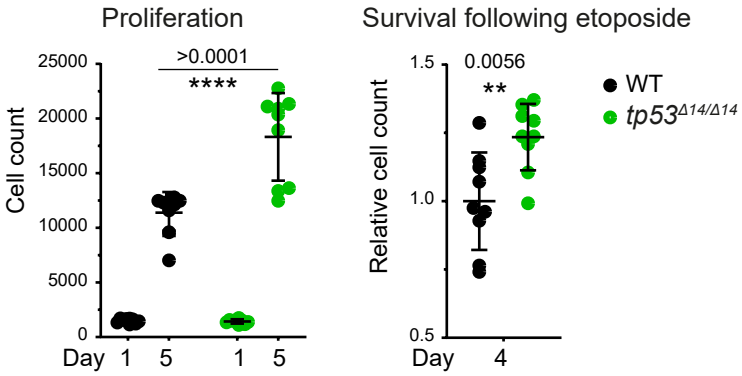

Acknowledgements

We thank the Harel lab for stimulating discussion and feedback on the manuscript. We thank Yonatan Birnbaum, Fatma Idrees, and Reem Barakat for killifish maintenance, and Naomi Melamed-Book from the imaging facility (HUJI). Supported by the ERC StG #101078188 (I.H.), Zuckerman Program (I.H.), ISF 2178/19 (I.H.), Israeli Ministry of Science 3-17631 (I.H.), 3-16872 (I.H.), the Moore Foundation GBMF9341 (I.H.), BSF-NSF 2020611 (I.H.), the Israeli Ministry of Agriculture 12-16-0010 (I.H), the Levi Eshkol scholarship of the Israeli Ministry of Science (E.M), the Czech Science Foundation (#22-01781O), and the Ministry of Education, Youth and Sports of the Czech Republic (#CZ.02.1.01/0.0/0.0/16_025/0007370) (R.F.), the Pamela and Paul Austin Research Center on Aging fellowship (T.A.). B.R. was supported by the Israel Science Foundation (ISF), grant numbers: 1416/19 and 2841/19, and also received funding from a HFSP grant (RGY0085/2019).

Author contributions

I.R., R.F., E.M., and I.H. designed the study. I.R., R.F. and E.M., performed experiments, I.R. generated the *Killibow* transgenic line. H.C. generated the *rag2* mutant. M.B. and G.A. generated the *atm* mutant. M.D. generated and characterized the *tp53* mutant. T.A. designed and performed the analysis of the kidney RNA-seq of *rag2* mutants under the supervision of I.H.. A.O.G. generated the *Killibow* cell line and performed experiments using this cell line. B.R., and I.H. performed and analyzed the phagocytosis assays. I.R., R.F., E.M., and I.H. wrote the manuscript. All authors commented on the manuscript.

Ethics declaration

The authors declare no competing interests.

RESOURCE AVAILABILITY

Material availability

Plasmids and corresponding annotated maps are available via Addgene (#47929, #13776, #118219, #224713, #31823). PCS2FA is available from Kawakami, K. (kokawaka@lab.nig.ac.jp). All fish lines are available upon request.

Data and Code availability

All raw RNA sequencing data, as well as processed datasets could be found in the GEO database, accession number GSE226279. The code is available in the GitHub repository for this paper https://github.com/Harel-lab/Killibow-rag2-mutant.

Data analysis

In the melanoma experiments, fish were excluded from further analysis if they died during the experiment, see **Table S2**. Otherwise, no data was excluded. We assumed normality for all data (as common for traits such as tumor size, color diversity etc.). We used a Student's t-test for comparing 2 groups, and an ANOVA test for more than 2 groups. To compare distributions between 2 groups we used Fisher's exact test. For biological replicates, we used parallel measurements of individual fish that capture random variation. Replicates were considered technical when the same experiment was conducted several times. All experiments were replicated at least twice. For melanoma experiments, fish were randomly selected for engraftment from age-matched cohorts. Visual scoring of melanoma presence and size was blindly and independently performed by two researchers. Power analysis was performed for melanoma experiments, predicting a reduction of 50% in engraftment success with an alpha of 0.05 and power of 80%:

$$k=\frac{n_2}{n_1}=1$$

$$n_1 = \frac{(\sigma_1^2 + \sigma_2^2/k)(z_{1-\frac{\alpha}{2}} + z_{1-\beta})^2}{\Delta^2}$$

$$n_1 = \frac{\left(5^2 + \frac{5^2}{1}\right)(1.96 + 0.84)^2}{12.5^2}$$

$$n_1 = 3$$

$$n_2 = kn_1 = 3$$

EXPERIMENTAL MODEL AND SUBJECT DETAILS

African turquoise killifish strain, husbandry, and maintenance

The African turquoise killifish (GRZ strain) were housed as previously described[20,88]. Fish were grown at 28 °C in a central filtration recirculating system with a 12 h light/dark cycle at the Hebrew University of Jerusalem (Aquazone ltd, Israel). Fish were fed once a day with live Artemia until the age of 2 weeks (#109448, Primo), and starting week 3, fish were fed three times a day on weekdays (and once a day on weekends), with GEMMA Micro 500 Fish Diet (Skretting Zebrafish, USA), supplemented with Artemia twice a day. All turquoise killifish care and uses were approved by the Subcommittee on Research Animal Care at the Hebrew University of Jerusalem (IACUC protocols #NS-18-15397-2 and #NS-22-16915-3).

CRISPR/Cas9 target prediction and gRNA synthesis

CRISPR/Cas9 genome-editing protocols were performed according to published protocols[20,88]. In brief, for gene targeting, a gRNA target site was identified using CHOPCHOP (https://chopchop.rc.fas.harvard.edu/)[100], chosen gRNAs are listed below. Design of variable oligonucleotides, and hybridization with a universal reverse oligonucleotide was performed according to[20], and the resulting products were used as a template for *in vitro* transcription. Each gRNA was *in-vitro* transcribed and purified using TranscriptAid T7 High Yield Transcription Kit (Thermo Scientific #K0441), according to the manufacturer's protocol.

Gene name	**gRNA sequence**
rag2 (Exon 1, XM_015964119.1)	GGGAGTTACATCATTCACGGCGG
	GGGTCTCACAAGAAAGCAAGGGG
tp53 (Exon 3, NM_001323800.1)	GATGGGTGGTGACTCCAAAGCGG
atm (Exon 2, XM_015951840.2)	GGTGCGATCCAATTCCTGCATGG

Production of Cas9 and transposase mRNA

Experiments were performed according to[15,20,88]. The pCS2-nCas9n expression vector was used to produce *Cas9* mRNA (Addgene, #47929)[101], and the PCS2FA plasmid was used to produce transposase mRNA[102]. PCS2FA is available from Kawakami, K. (kokawaka@lab.nig.ac.jp). Capped and polyadenylated mRNA was *in-vitro* transcribed and purified using the mMESSAGE mMACHINE SP6 ULTRA (ThermoFisher # AM1340).

Production of *Cre* mRNA

A *Cre-gfp* DNA cassette was amplified from pCAG-*Cre*:*gfp* (Addgene #13776) using a forward primer (CreF: TGAGCCGCCACCATGGC), and M13 reverse primer (M13R: CAGGAAACAGCTATGAC). An SP6 promoter was then added by a second round of amplification using the following forward primer: (SP6F: CCCTAGGTATTTAGGTGACACTATAGTGAGCCGCCACCATGGC). PCR products were sequence verified and purified using standard methods. The clean SP6-*Cre-gfp* cassette was then used as a template for *in-vitro* RNA transcription. Capped and polyadenylated mRNA was *in-vitro* transcribed and purified using the mMESSAGE mMACHINE SP6 ULTRA (ThermoFisher # AM1340).

Microinjection of turquoise killifish embryos

For generation of the mutant fish using CRISPR/Cas9, microinjection of turquoise killifish embryos was performed according to[20]. Briefly, nCas9n-encoding mRNA (300 ng/µL) and gRNA (30 ng/µL) were mixed with phenol-red (P0290, Sigma-Aldrich) and co-injected into two-cell stage fish embryos. Sanger DNA sequencing was used for detecting successful germline transmission on F1 embryos using the following primer sequences: *rag2F*: TGATGTTTTCTGTTTTGACCCA and *rag2R*: TATCTGTGGGCAGGACCTGTA. *Tp53F*: ACTCTGCTTTGGACTTGGAGAG and *tp53R*: GCTTACCAATAAAGGCATTTGGCTC, *atmF*: CTGAGGGTGTGGTCTGATAGC and *atmR*: TCTCCTTCTGGAGGTAACGC.

Fish with desired alleles were further outcrossed to minimize potential off-target effects, and maintained as stable lines. For generation of transgenic *Killibow* fish using Tol2, transposase-encoding mRNA (300 ng/µL) and the *Zebrabow* vector (30 ng/µL, Addgene #118219) were co-injected into one-cell stage fish embryos as described above. Successful germline transmission on F1, and selection of founders was performed according to the uniformity and intensity of the RFP signal.

Estimation of transgene copy number in the *Killibow*

In order to estimate the copy number of the *Killibow* transgene in the killifish genome we performed real time qPCR as previously described[46,47], using genomic DNA (gDNA) extracted from cultured fibroblasts from WT and *Killibow* fish. gDNA was extracted using a standard gDNA extraction kit (QIAGEN #56304) according to the manufacturer instructions. qPCR was performed using Fast SYBR Green Master Mix (ThermoFisher scientific # 4385612) on a Mic qPCR Cycler (Bio Molecular Systems). The *Killibow* transgenic construct was compared to a reference gene, Cyclin Dependent Kinase Inhibitor 2A/B (p16), using the following primers: *p16-F*: ATCTCGAAGGCAAGCATCC, *p16-R*: GCAGAAGCGACTCCACATC, *Killibow-F*: TTCATGTACGGCTCCAAGGC, *Killibow-R*: ACCTTGTAGATCAGCGTGCC). Copy number was determined using the following equation: relative *Killibow* copy number per diploid cell= $2\times2^{-\Delta\Delta Cq}$, where ΔΔCq is $(Cq^{Killibow}-Cq^{p16})_{Killibow\ cells} - (Cq^{Klilibow}-Cq^{p16})_{GRZ\ cells}$. We found a ~24-fold difference between our reference gene and the *Killibow* construct.

METHOD DETAILS

Tail regeneration

Regeneration protocols were adapted from[48]. Briefly, one-month or four-month-old fish were sedated in MS222 (200 mg/L Tricaine), placed on a damp kimwipe, and approximately 50% of their tail was amputated using a square razor blade with one clean cut. Pictures were taken

using a Leica MC190HD camera mounted on a Leica stereomicroscope, before and after amputation, and every 3 days for 18 days.

Depletion of endogenous spermatogenesis and spermatogonial stem cell transplantation

This protocol was adapted from zebrafish[49]. Briefly, young killifish males (6 weeks old) were kept at 28 °C, with a daily temperature increase of 1 °C for seven days, until reaching 34 °C. Fish were kept at 34 °C for one week, weighed and received a single intraperitoneal injection of 40 mg/kg of busulfan (ENZO) dissolved in DMSO. At each step of the protocol, testes (from n=4 individuals for each step) were sampled, fixed, paraffin embedded, sectioned, and stained for DDX4. Specifically, we used an anti-DDX4 primary antibody (Abcam #13840, 1:300 dilution) and a donkey anti-rabbit secondary antibody (Abcam #150064, 1:500 dilution). For donor cell preparation, testes from one male were minced with scissors, digested with 0.2% Collagenase Type P (Merck Millipore) and 0.12% Dispase II (Sigma Aldrich) in Leibovitz's L-15 Medium (Gibco) for 60 min at RT. Cells were then filtered using a Falcon 40 µm filter, centrifuged at 0.4g for 10 min and resuspended in L15 with 10% FBS. The suspension of spermatogonial stem cells was mixed with phenol red and transplanted into the testes through the genital pore (2 µL per fish), using a glass capillary needle coupled to a pneumatic microinjector. One month following transplantation, gonads were removed and imaged.

Generation of the *Killibow* cell-line

Cells were isolated as described previously[88]. Briefly, adult fish were sedated with MS-222 (200 mg/L Tricaine), and a 2–3 mm piece of their tail fin was trimmed using a sterile razor blade. Following disinfection with 70% ethanol, tissue samples were incubated for 2 h with 1 mL of an antibiotic solution containing Gentamicin (50 µg/mL Gibco) and Primocin™ (50 µg/mL, InvivoGen) in PBS at room temperature. Tissues were then transferred into an enzymatic digestion buffer (200 µL, in a 24-well plate) containing Dispase II (2 mg/mL, Sigma Aldrich) and Collagenase Type P (0.4 mg/mL, Merck Millipore) in Leibovitz's L-15 Medium (Gibco), minced with a sterile pair of scissors and incubated for 15 min. The digested tissue was then mixed with 400 µL of complete Leibovitz's L-15 growth medium (Gibco), supplemented with Fetal Bovine Serum (15% FBS, Gibco), penicillin/streptomycin (50 U/ml, Gibco), Gentamicin (Gibco, 50 µg/ml) and Primocin™ (50 µg/ml, InvivoGen). On the following day, media was carefully replaced, and during the first 7 days, cells were daily washed with fresh media before adding new media. When cells reached 85–90% confluency, they were passaged with Trypsin-EDTA 0.05% (0.25% Trypsin-EDTA, diluted in PBS). Cells

were incubated in a 28 °C humidified incubator (Binder, Thermo Scientific) with normal air composition, and were passaged for ~20 passages.

Plasmid transfection and Doxycycline treatment

Killibow cells were co-transfected with a transposase-encoding plasmid (Addgene #31823) and a Tol2 Doxycycline-inducible *Cre* plasmid that contains a puromycin resistance cassette (Addgene #224713). Transfection was performed using Lipofectamine 3000 (Invitrogen #L3000001) according to the manufacturer's instructions. Transfected cells were enriched using 10µg/ml Puromycin (InvivoGen #ant-pr) for 2 weeks. Following selection, cells were treated with 100 ng/ml Doxycycline (Sigma-Aldrich #D5207) for 48 hours, washed with fresh media, and immediately imaged.

Plasmid electroporation

Electroporation was performed as previously described[19]. Briefly, 5 µl of a solution containing a *Cre-gfp* plasmid (~2 µg/µl, Addgene #13776) and 0.1% phenol red (Sigma #P0290) was injected intramuscularly using a Nanofil syringe (WPI, #NANOFIL). Fish were then electroporated using 7 mm tweezer electrodes (NEP GENE #CUY650P10) with the ECM 830 generator. (BTX #45-0661). Electrodes were coated with wet cotton to minimize the risk to the fish. Fish were electroporated with 6 pulses of 28 V, for 60 ms each with an interval of 1 s between each pulse. Images were recorded by a Leica MC190HD camera mounted on a Leica M165FC stereomicroscope.

Cell transplantation

For transplantation of fibroblasts, *Killibow* cells were isolated from the tail, made into a cell line as described above and were injected into *rag2* homozygous fish (40,000 cells/µl, at 4 µl per fish). For the injection, adult male recipient fish (~1.5-month-old) were anesthetized, and intramuscular injection was performed using a Nanofil syringe (WPI, #NANOFIL).

For transplantation of melanoma-like cells, an 8-month-old male with a melanocyte expansion in the tail fin (**Figure 4a**) was euthanized, part of the fin was dissected, finely minced with scissors and digested with 0.2% Collagenase Type P (Merck Millipore) and 0.12% Dispase II (Sigma Aldrich) in Leibovitz's L-15 Medium (Gibco) for 30 min at RT. Cells were filtered using a Falcon 40 µm filter, centrifuged at 0.4g for 10 min and resuspended in L15 with 10% FBS and injected dorsally in *rag2* and WT recipients. Following *in-vivo* expansion of the melanoma cells in the *rag2* recipients, muscle tissue containing melanoma was dissected and prepared for transplantation into recipients again as described above. Fish were then

monitored, and melanoma development was scored visually 5 weeks post injection. Further passages were derived from dorsal muscle of melanoma injected fish as described above.

Immune cell preparation

Functional analysis of the killifish immune system was adapted from previous studies[78,103]. Young and old killifish, ages 2 and 5 months respectively, were euthanized before blood and kidney collection. Blood was obtained by tail amputation and collected with a micropipette tip coated with heparin. Kidney was dissected and placed into ice-cold 0.9× PBS containing 5% FBS. Single-cell suspensions were generated by mechanical dissociation, followed by passage through a 40 µm cell strainer for obtaining a single cell suspension. All cells were kept on ice in 0.9X Phosphate Buffered Saline (PBS), supplemented with 5% FBS.

GIEMSA staining

Cytospin preparations were made following centrifugation at 300 rpm for 3 min onto glass slides in a Cytospin cytocentrifuge (Shandon). Cytospin preparations were processed through Giemsa stains (Fluka) for morphological analyses.

Flow cytometry

Cells were washed and resuspended in ice-cold 0.9× PBS plus 5% FBS and were passed through a filter with a 40-µm mesh. Propidium iodide (PI, Sigma) was added to a concentration of 1 µg/ml to exclude dead cells and debris. Flow cytometry sorting was based on PI exclusion, forward scatter and side scatter with a FACS-Influx (Beckton Dickinson), and analysis with LSR-II flow cytometer (10,000cells per sample). Analysis was performed using FlowJo V10.

Phagocytosis

For beads phagocytosis assays, cells were incubated with Fluoresbrite Yellow-Green carboxylate microspheres (1 µm) for 3 hr at 26 °C in a ratio of 1:1, beads to cells, prior to analysis by flow cytometry. Cells were co-stained with either LysoTracker® deep red (75 nM, Thermo Fisher Scientific) or DiI (Thermo Fisher Scientific) for the analysis of double positive for phagocytosis. For confocal analysis of validation of phagocytosis, positive cells were sorted by BD FACS AriaII flow cytometer and placed on ibidi µ-Slide 18 wells poly-L-lysine coated overnight at 4 °C. Confocal images were obtained with an LSM 700 confocal microscope (Carl Zeiss). The 3D confocal analysis was performed on Z-stack images from green and red channels using surface analysis of the volumes. To generate the images, the Z-axis was lowered to visualize inside the cells, including the green beads as was previously shown[103].

Cryosectioning

Fish were euthanized and dissected as described above. Tissues were fixed in 4% PFA at 4 °C for 2 hours and immersed in a 30% sucrose (Bio-Lab #001922059100) solution for 2 hours at 4 °C followed by immersion in OCT (Scigen Scientific Gardena #4586) at 4°C overnight and frozen in liquid nitrogen. All immersions were performed with mild shaking. Serial 10 µm sections were taken using a cryostat, airdried, and mounted with Fluoroshield (Sigma-Aldrich # F6182). Samples were imaged using a fully motorized Olympus IX83 microscope with a Photometrics BSI camera and processed in imageJ[65].

Hematoxylin and eosin

Tissues samples were processed as described previously[14,15,106–112,17,19,20,51,88,91,104,105]. Briefly, fish were euthanized with 500 mg/l tricaine (MS222, #A5040, Sigma). The body cavity of the fish was opened and fixed for 72 h in 4% PFA solution at 4 °C. Samples were dehydrated and embedded in paraffin using standard procedures. Sections of 5-10 µm were stained with Hematoxylin and Eosin and examined by microscopy. A fully motorized Olympus IX83 microscope with an Olympus DP28 camera was used to collect images.

Fluorescence microscopy

Organs were dissected on ice and imaged using a fluorescent binocular stereomicroscope (Leica MC190HD camera mounted on a Leica M165FC stereomicroscope). For live imaging of cell, cells were plated on a µ-Slide 8 Well Glass Bottom plates (ibidi, #80827). For imaging of live cells, either a laser scanning confocal microscope (FV-1200, Olympus, Japan), or a fully motorized Olympus IX83 microscope with an Olympus DP28 camera was used.

Color profiling of *Killibow* images

Color spectra profiling in *Killibow* was done according to[23] with slight modifications. Individual RGB values for areas that displayed a single color from the acquired images of cells, embryos, muscle tissue sections, and transplanted testis were measured in FIJI, converted to hue and saturation values and plotted on a Hue-Saturation plot.

EdU staining

A male fish that has been previously injected with a third-passage melanoma then received an IP injection of EdU (50mg/kg in DMSO). After 6 hours the fish was sacrificed, its trunk was dissected, fixed for 48 h in 4% formaldehyde at 4 °C, dehydrated in an ethanol and chloroform series, embedded in paraffin, and sectioned. Consecutive 7 µm sections were collected

696 individually on slides, deparaffinized and rehydrated. One section was immediately stained
697 with the EdU-Click Kit (baseclick BCK-EdU488IM100) and mounted with Fluoroshield
698 containing DAPI. An adjacent section was treated overnight with 30% H_2O_2 to bleach the
699 pigment of the melanoma (according to[113]), and then stained with the EdU-Click Kit and
700 mounted with Fluoroshield containing DAPI. Imaging was performed as described above.

701 **Profiling of V(D)J recombination**

702 Amplification of the V(D)J locus was performed according to[38], with slight modifications.
703 RNA was collected from the kidneys of 3 WT and 3 *rag2* mutant males and purified using the
704 Direct-zol RNA Miniprep kit (Zymo Research, #R5052). Forty-five ng of RNA was combined
705 with 2 µl of 10 µM gene-specific primer (GSP, **Table S3**), homologous with the second
706 constant-region exon of N. furzeri IgHM. The reaction volume was brought to a total of 8 µl
707 with nuclease-free water, and the resulting mixture was incubated for 2 min at 70 °C to denature
708 the RNA, then cooled to 42 °C to anneal the GSP[114].

709 Following annealing, the RNA-primer mixture was combined with 12 µl of reverse
710 transcription master-mix (SMARTScribe Reverse Transcriptase, Takara-Clontech #639538)
711 including the reverse-transcriptase enzyme and template-switch adapter SmartNNNa primer
712 (**Table S3**). This primer consists of a constant sequence used for further PCR steps, a variable
713 sequence containing multiple random nucleotides (N) that function as a unique molecular
714 identifier (UMI) and several deoxyuridine bases (U), which are used to degrade the primer
715 following amplification and a 3'-terminal sequence of riboguanosine residues, which anneal to
716 cytidine residues added by the reverse transcriptase and enable template switching (See **Figure**
717 **3c**). The complete reaction mixture was incubated for 1 h at 42 °C for the reverse transcription
718 reaction, then mixed with 2 µl of uracil DNA glycosylase (NEB, #M0280S, 1000 units) and
719 incubated for a further 40 min at 37 °C to digest the template-switch adapter.

720 Following reverse transcription, the reaction product was purified using a standard PCR
721 purification kit (QIAGEN #28104). The reaction mixture then underwent PCR amplification
722 with the PCRBio HS Taq Mix Red (#PB10.23) using the IGH-B and M1SS primers (**Table**
723 **S3**), according to the manufacturer's instructions and ran on a 1% agarose gel.

724 **RNA-seq library preparation**

725 Head kidney was isolated as described previously[20]. Samples were disrupted by bead beating
726 in 300 µl of TriZol (Sigma) and a single 3 mm metal bead (Eldan, BL6693003000) using
727 TissueLyzer LT (QIAGEN, #85600) with a dedicated adaptor (QIAGEN, #69980). Beating

was performed at 50 Hz for 5 min. RNA extraction was performed with TRI Reagent (Sigma, #T9424) RNA concentration and quality were determined by using an Agilent 2100 bioanalyzer (Agilent Technologies). Library preparation was performed using KAPA mRNA HyperPrep Kit (ROCHE-08105936001) according to the recommended protocols. Library quantity and pooling were measured by Qubit (dsDNA HS, Q32854), size selection at 4% agarose gel. Library quality was measured by Tape Station (HS, 5067-5584). Libraries were sequenced by NextSeq 2000 P2, 100 cycle,75 bp single-end (Illumina, 20024906) with ~40 million reads per sample.

RNA sequencing analysis

Quality control and adapter trimming of the fastq sequence files were performed with FastQC (v0.11.8)[115], fastx-toolkits (v0.0.13), Trim Galore! (v0.6.4)[116], and Cutadapt (3.4)[117]. Options were set to remove Illumina TruSeq adapters and end sequences to retain high-quality bases with *phred* score > 20 and a remaining length > 20 bp. Successful processing was verified by re-running FastQC. Reads were mapped and quantified to the killifish genome Nfu_20140520 [17,18] using STAR 2.7.6a[118]. Differential gene expression between *rag2* mutant and WT fish was performed using the edgeR package, (v3.32.1)[119,120] by the classic model (exactTest function).

Gene Ontology Enrichment Analysis

Enriched Gene Ontology (GO) terms associated with transcripts level was identified using GO implemented in R package clusterProfiler (v3.18.1)[121] with the threshold of FDR < 0.05 and log2(FC) > 1. GO terms were based on human GO annotations from org.Hs.eg.db (v3.13.0) [122] and AnnotationDbi (v1.54.1)[123].

Cell Growth and apoptosis

For growth measurement, 3 WT and 3 *tp53*$^{\Delta 14/\Delta 14}$-derived primary cultures were seeded with 1000 cells/well (12-well plates). At Days 1 and Day 5 cells were trypsinized, resuspended, and counted using CellDrop™ (DeNovix). For apoptosis evaluation, the same biological replicates were seeded at 5000 cells/well. On the next day, cells were treated with 500 µM Etoposide (Sigma # E1383), which arrested cell proliferation, and cell numbers were counted on day 4 post-treatment.

References:

1. Radtke, F. & Clevers, H. Self-renewal and cancer of the gut: two sides of a coin. *Science (80-.).* **307**, 1904–1909 (2005).
2. Rossi, D. J., Jamieson, C. H. M. & Weissman, I. L. Stems cells and the pathways to aging and cancer. *Cell* **132**, 681–696 (2008).
3. Sharpless, N. E. & DePinho, R. A. How stem cells age and why this makes us grow old. *Nat. Rev. Mol. cell Biol.* **8**, 703–713 (2007).
4. Lopez-Otin, C. *et al.* The hallmarks of aging. *Cell* **153**, 1194–1217 (2013).
5. Niccoli, T. & Partridge, L. Ageing as a risk factor for disease. *Curr Biol* **22**, R741-52 (2012).
6. Fane, M. & Weeraratna, A. T. How the ageing microenvironment influences tumour progression. *Nat. Rev. Cancer* **20**, 89–106 (2020).
7. Lawson, D. A., Kessenbrock, K., Davis, R. T., Pervolarakis, N. & Werb, Z. Tumour heterogeneity and metastasis at single-cell resolution. *Nat. Cell Biol.* **20**, 1349–1360 (2018).
8. Jackson, H. W. *et al.* The single-cell pathology landscape of breast cancer. *Nature* **578**, 615–620 (2020).
9. Kinker, G. S. *et al.* Pan-cancer single-cell RNA-seq identifies recurring programs of cellular heterogeneity. *Nat. Genet.* **52**, 1208–1218 (2020).
10. Hernandez-Segura, A. *et al.* Unmasking transcriptional heterogeneity in senescent cells. *Curr. Biol.* **27**, 2652–2660 (2017).
11. Cohn, R. L., Gasek, N. S., Kuchel, G. A. & Xu, M. The heterogeneity of cellular senescence: insights at the single-cell level. *Trends Cell Biol.* (2022).
12. Kimmel, J. C. *et al.* Murine single-cell RNA-seq reveals cell-identity-and tissue-specific trajectories of aging. *Genome Res.* **29**, 2088–2103 (2019).
13. Consortium, T. M., h, O. coordination S. N. 1 K. J. 2 N. N. F. 2 M. A. P. 2 Q. S. R. quake@ stanford. edu 2 3 f W.-C. T. twc@ stanford. edu 4 5 6 g D. S. spyros. darmanis@ czbiohub. org 2, 3, L. coordination B. J. 2 B. O. 2 C. M. B. 3 C. S. 2 G. F. 2 J. R. C. 3 M. A. 2 P. L. 2 P. A. O. 2 S. R. V. 2 S. G. M. 3 W. J. T. 2 Z. F. & 3, C. data analysis B. J. 2 B. O. 2 C. P. 2 C. D. 3 D. S. 2 D. J. L. 2 27 K. J. 2 P. A. O. 2 S. G. M. 3 W. J. T. 2 Z. F. Single-cell transcriptomics of 20 mouse organs creates a Tabula Muris. *Nature* **562**, 367–372 (2018).
14. Harel, I. *et al.* A platform for rapid exploration of aging and diseases in a naturally short-lived vertebrate. *Cell* (2015) doi:10.1016/j.cell.2015.01.038.
15. Harel, I., Valenzano, D. R. & Brunet, A. Efficient genome engineering approaches for the short-lived African turquoise killifish. *Nat. Protoc.* (2016) doi:10.1038/nprot.2016.103.
16. Cui, R. *et al.* Relaxed Selection Limits Lifespan by Increasing Mutation Load. *Cell* **178**, 385-399 e20 (2019).
17. Valenzano, D. R. *et al.* The African Turquoise Killifish Genome Provides Insights into Evolution and Genetic Architecture of Lifespan. *Cell* **163**, 1539–1554 (2015).
18. Reichwald, K. *et al.* Insights into Sex Chromosome Evolution and Aging from the

Genome of a Short-Lived Fish. *Cell* **163**, 1527–1538 (2015).

19. Moses, E., Franek, R. & Harel, I. A scalable and tunable platform for functional interrogation of peptide hormones in fish. *Elife* **12**, e85960 (2023).

20. Astre, G., Moses, E. & Harel, I. The African turquoise killifish (Nothobranchius furzeri): biology and research applications. in *Laboratory Fish in Biomedical Research* 245–287 (Elsevier, 2022).

21. Harel, I. The turquoise killifish. *Nat. Methods* (2022) doi:10.1038/s41592-022-01631-y.

22. Platzer, M. & Englert, C. Nothobranchius furzeri: A Model for Aging Research and More. *Trends Genet* **32**, 543–552 (2016).

23. Pan, Y. A. *et al.* Zebrabow: multispectral cell labeling for cell tracing and lineage analysis in zebrafish. *Development* **140**, 2835–2846 (2013).

24. Wagner, D. E. & Klein, A. M. Lineage tracing meets single-cell omics: opportunities and challenges. *Nat. Rev. Genet.* **21**, 410–427 (2020).

25. Baron, C. S. & van Oudenaarden, A. Unravelling cellular relationships during development and regeneration using genetic lineage tracing. *Nat. Rev. Mol. cell Biol.* **20**, 753–765 (2019).

26. VanHorn, S. & Morris, S. A. Next-generation lineage tracing and fate mapping to interrogate development. *Dev. Cell* **56**, 7–21 (2021).

27. Aghaallaei, N. *et al.* Identification, visualization and clonal analysis of intestinal stem cells in fish. *Dev.* **143**, (2016).

28. Centanin, L. *et al.* Exclusive multipotency and preferential asymmetric divisions in post-embryonic neural stem cells of the fish retina. *Dev.* **141**, (2014).

29. Tsai, S. L., Villaseñor, S., Shah, R. R. & Galloway, J. L. Endogenous tenocyte activation underlies the regenerative capacity of the adult zebrafish tendon. *npj Regen. Med.* **8**, (2023).

30. Henninger, J. *et al.* Clonal fate mapping quantifies the number of haematopoietic stem cells that arise during development. *Nat. Cell Biol.* **19**, (2017).

31. Livet, J. *et al.* Transgenic strategies for combinatorial expression of fluorescent proteins in the nervous system. *Nature* **450**, 56–62 (2007).

32. Jordan, C. T., Guzman, M. L. & Noble, M. Cancer stem cells. *N. Engl. J. Med.* **355**, 1253–1261 (2006).

33. Reya, T., Morrison, S. J., Clarke, M. F. & Weissman, I. L. Stem cells, cancer, and cancer stem cells. *Nature* **414**, 105–111 (2001).

34. Patton, E. E., Zon, L. I. & Langenau, D. M. Zebrafish disease models in drug discovery: from preclinical modelling to clinical trials. *Nat. Rev. Drug Discov.* **20**, 611–628 (2021).

35. Couëdel, C. *et al.* Analysis of mutations from SCID and Omenn syndrome patients reveals the central role of the Rag2 PHD domain in regulating V (D) J recombination. *J. Clin. Invest.* **120**, 1337–1344 (2010).

36. Villa, A. *et al.* V (D) J recombination defects in lymphocytes due to RAG mutations: severe immunodeficiency with a spectrum of clinical presentations. *Blood, J. Am. Soc.*

Hematol. **97**, 81–88 (2001).

37. Tang, Q. *et al.* Optimized cell transplantation using adult rag2 mutant zebrafish. *Nat. Methods* **11**, 821–824 (2014).

38. Bradshaw, W. J., Poeschla, M., Placzek, A., Kean, S. & Valenzano, D. R. Extensive age-dependent loss of antibody diversity in naturally short-lived turquoise killifish. *Elife* **11**, (2022).

39. Press, C. M. & Evensen, Ø. The morphology of the immune system in teleost fishes. *Fish Shellfish Immunol.* **9**, 309–318 (1999).

40. Oh, J., Magnuson, A., Benoist, C., Pittet, M. J. & Weissleder, R. Age-related tumor growth in mice is related to integrin α 4 in CD8+ T cells. *JCI insight* **3**, (2018).

41. Mosimann, C. *et al.* Ubiquitous transgene expression and Cre-based recombination driven by the ubiquitin promoter in zebrafish. *Development* **138**, 169–177 (2011).

42. Dolfi, L., Ripa, R., Antebi, A., Valenzano, D. R. & Cellerino, A. Cell cycle dynamics during diapause entry and exit in an annual killifish revealed by FUCCI technology. *Evodevo* **10**, 29 (2019).

43. Kratochwil, C. F., Sefton, M. M., Liang, Y. & Meyer, A. Tol2 transposon-mediated transgenesis in the Midas cichlid (Amphilophus citrinellus)—towards understanding gene function and regulatory evolution in an ecological model system for rapid phenotypic diversification. *BMC Dev. Biol.* **17**, 1–11 (2017).

44. Stahl, B. A. *et al.* Stable transgenesis in Astyanax mexicanus using the Tol2 transposase system. *Dev. Dyn.* **248**, 679–687 (2019).

45. Chen, Y. R. *et al.* Tissue-specific landscape of protein aggregation and quality control in an aging vertebrate. *Dev. Cell* (2024) doi:https://doi.org/10.1016/j.devcel.2024.04.014.

46. Hartmann, N. *et al.* Mitochondrial DNA copy number and function decrease with age in the short-lived fish Nothobranchius furzeri. *Aging Cell* (2011) doi:10.1111/j.1474-9726.2011.00723.x.

47. Paugh, B. S. *et al.* Reference standards for accurate validation and optimization of assays that determine integrated lentiviral vector copy number in transduced cells. *Sci. Rep.* **11**, (2021).

48. Wendler, S., Hartmann, N., Hoppe, B. & Englert, C. Age-dependent decline in fin regenerative capacity in the short-lived fish Nothobranchius furzeri. *Aging Cell* **14**, 857–866 (2015).

49. Nobrega, R. H. *et al.* Spermatogonial stem cell niche and spermatogonial stem cell transplantation in zebrafish. *PLoS One* **5**, e12808 (2010).

50. Fijak, M. & Meinhardt, A. The testis in immune privilege. *Immunol. Rev.* **213**, 66–81 (2006).

51. Moses, E. *et al.* The killifish germline regulates longevity and somatic repair in a sex-specific manner. *Nat. Aging* 1–23 (2024).

52. Rozenberg, I., Moses, E. & Harel, I. CRISPR–Cas9 Genome Editing in Nothobranchius furzeri for Gene Knockout and Knock-In. *Cold Spring Harb. Protoc.* (2022).

53. Hao, Z. & Rajewsky, K. Homeostasis of peripheral B cells in the absence of B cell

influx from the bone marrow. *J. Exp. Med.* **194**, 1151–1164 (2001).

54. Cannon, J. P. *et al.* A bony fish immunological receptor of the NITR multigene family mediates allogeneic recognition. *Immunity* **29**, 228–237 (2008).

55. Yoder, J. A. Form, function and phylogenetics of NITRs in bony fish. *Dev. Comp. Immunol.* **33**, 135–144 (2009).

56. Renshaw, S. A. & Trede, N. S. A model 450 million years in the making: zebrafish and vertebrate immunity. *Dis Model Mech* **5**, 38–47 (2012).

57. Moore, F. E. *et al.* Single-cell transcriptional analysis of normal, aberrant, and malignant hematopoiesis in zebrafish. *J. Exp. Med.* **213**, 979–992 (2016).

58. Carmona, S. J. *et al.* Single-cell transcriptome analysis of fish immune cells provides insight into the evolution of vertebrate immune cell types. *Genome Res.* **27**, 451–461 (2017).

59. Pereiro, P. *et al.* Zebrafish Nk-lysins: first insights about their cellular and functional diversification. *Dev. Comp. Immunol.* **51**, 148–159 (2015).

60. Dornburg, A. & Yoder, J. A. On the relationship between extant innate immune receptors and the evolutionary origins of jawed vertebrate adaptive immunity. *Immunogenetics* 1–18 (2022).

61. Yoder, J. A. *et al.* Resolution of the novel immune-type receptor gene cluster in zebrafish. *Proc. Natl. Acad. Sci.* **101**, 15706–15711 (2004).

62. Bradshaw, W. J. & Valenzano, D. R. Extreme genomic volatility characterizes the evolution of the immunoglobulin heavy chain locus in cyprinodontiform fishes. *Proc Biol Sci* **287**, 20200489 (2020).

63. Di Cicco, E., Tozzini, E. T., Rossi, G. & Cellerino, A. The short-lived annual fish Nothobranchius furzeri shows a typical teleost aging process reinforced by high incidence of age-dependent neoplasias. *Exp Gerontol* **46**, 249–256 (2011).

64. Dyková, I. *et al.* Histopathology of laboratory-reared Nothobranchius fishes: Mycobacterial infections versus neoplastic lesions. *J. Fish Dis.* **44**, 1179–1190 (2021).

65. Hu, C. K. & Brunet, A. The African turquoise killifish: A research organism to study vertebrate aging and diapause. *Aging Cell* (2018) doi:10.1111/acel.12757.

66. Sato, Y. *et al.* Tumorigenicity assessment of cell therapy products: The need for global consensus and points to consider. *Cytotherapy* **21**, 1095–1111 (2019).

67. Amatruda, J. F. & Patton, E. E. Genetic models of cancer in zebrafish. *Int Rev Cell Mol Biol* **271**, 1–34 (2008).

68. Storer, N. Y. & Zon, L. I. Zebrafish models of p53 functions. *Cold Spring Harb. Perspect. Biol.* **2**, a001123 (2010).

69. Muller, P. A. J. & Vousden, K. H. p53 mutations in cancer. *Nat. Cell Biol.* **15**, 2–8 (2013).

70. Oren, M. Decision making by p53: life, death and cancer. *Cell Death Differ.* **10**, 431–442 (2003).

71. Tokunaga, Y. *et al.* Comprehensive validation of T-and B-cell deficiency in rag1-null zebrafish: Implication for the robust innate defense mechanisms of teleosts. *Sci. Rep.* **7**, 7536 (2017).

72. García-Valtanen, P. *et al.* Zebra fish lacking adaptive immunity acquire an antiviral alert state characterized by upregulated gene expression of apoptosis, multigene families, and interferon-related genes. *Front. Immunol.* **8**, 121 (2017).

73. Bapat, S. A., Mali, A. M., Koppikar, C. B. & Kurrey, N. K. Stem and progenitor-like cells contribute to the aggressive behavior of human epithelial ovarian cancer. *Cancer Res.* **65**, 3025–3029 (2005).

74. Wegner, C. S. *et al.* Increasing aggressiveness of patient-derived xenograft models of cervix carcinoma during serial transplantation. *Oncotarget* **9**, 21036 (2018).

75. Castelo-Branco, C. & Soveral, I. The immune system and aging: a review. *Gynecol. Endocrinol.* **30**, 16–22 (2014).

76. Pang, W. W. *et al.* Human bone marrow hematopoietic stem cells are increased in frequency and myeloid-biased with age. *Proc. Natl. Acad. Sci.* **108**, 20012–20017 (2011).

77. Brunet, A., Goodell, M. A. & Rando, T. A. Ageing and rejuvenation of tissue stem cells and their niches. *Nat. Rev. Mol. Cell Biol.* **24**, 45–62 (2023).

78. Traver, D. *et al.* Transplantation and in vivo imaging of multilineage engraftment in zebrafish bloodless mutants. *Nat. Immunol.* **4**, 1238–1246 (2003).

79. Zapata, A. Ultrastructural study of the teleost fish kidney. *Dev. Comp. Immunol.* **3**, 55–65 (1979).

80. Tacutu, R. *et al.* Human Ageing Genomic Resources: new and updated databases. *Nucleic Acids Res* **46**, D1083–D1090 (2018).

81. Schartl, M. Beyond the zebrafish: diverse fish species for modeling human disease. *Dis Model Mech* **7**, 181–192 (2014).

82. Podrabsky, J. E., Riggs, C. L. & Wagner, J. T. Tolerance of Environmental Stress. in *Annual Fishes. Life History Strategy, Diversity, and Evolution* (eds. Berois, N., García, G. & De Sá, R. O.) 159–184 (CRC Press, Taylor & Francis, 2016). doi:10.1201/b19016.

83. Jaggard, J. B. *et al.* Cavefish brain atlases reveal functional and anatomical convergence across independently evolved populations. *Sci. Adv.* **6**, eaba3126 (2020).

84. Wang, W. *et al.* Changes in regeneration-responsive enhancers shape regenerative capacities in vertebrates. *Science (80-.).* **369**, (2020).

85. Antebi, A., Dolfi, L., Suen, T. K. & Ripa, R. Optimization of cryopreservation and in vitro fertilization techniques for the African turquoise killifish Nothobranchius furzeri. *bioRxiv* (2020).

86. Batlle, E. & Clevers, H. Cancer stem cells revisited. *Nat. Med.* **23**, 1124–1134 (2017).

87. Morabito, G. *et al.* Spontaneous onset of cellular markers of inflammation and genome instability during aging in the immune niche of the naturally short-lived turquoise killifish (Nothobranchius furzeri). *bioRxiv* 2002–2023 (2023).

88. Astre, G. *et al.* Genetic perturbation of AMP biosynthesis extends lifespan and restores metabolic health in a naturally short-lived vertebrate. *Dev. Cell* (2023).

89. Ripa, R. *et al.* Refeeding-associated AMPKγ1 complex activity is a hallmark of health and longevity. *Nat. Aging* **3**, 1544–1560 (2023).

90. Di Fraia, D. *et al.* A comprehensive atlas of the aging vertebrate brain reveals signatures of progressive proteostasis dysfunction. *bioRxiv* 2007–2023 (2023).

91. Harel, I. *et al.* Identification of protein aggregates in the aging vertebrate brain with prion-like and phase-separation properties. *Cell Rep.* 112787 (2024) doi:https://doi.org/10.1016/j.celrep.2023.112787.

92. Cooke, H. J. & Saunders, P. T. K. Mouse models of male infertility. *Nat. Rev. Genet.* **3**, 790–801 (2002).

93. Verhagen, M. M. M. *et al.* Clinical spectrum of ataxia-telangiectasia in adulthood. *Neurology* **73**, 430–437 (2009).

94. Aguado, J. *et al.* The Hallmarks of Aging in Ataxia-Telangiectasia. *Ageing Res. Rev.* 101653 (2022).

95. Haas, O. A. Primary immunodeficiency and cancer predisposition revisited: embedding two closely related concepts into an integrative conceptual framework. *Front. Immunol.* **9**, 3136 (2019).

96. Krug, J. *et al.* Generation of a transparent killifish line through multiplex CRISPR/Cas9mediated gene inactivation. *Elife* **12**, e81549 (2023).

97. Oginuma, M. *et al.* Rapid reverse genetics systems for Nothobranchius furzeri, a suitable model organism to study vertebrate aging. *Sci. Rep.* **12**, 11628 (2022).

98. Bedbrook, C. N., Nath, R. D., Nagvekar, R., Deisseroth, K. & Brunet, A. Rapid and precise genome engineering in a naturally short-lived vertebrate. *Elife* **12**, e80639 (2023).

99. Podrabsky, J. E. *et al.* Embryonic development of the annual killifish Austrofundulus limnaeus: An emerging model for ecological and evolutionary developmental biology research and instruction. *Dev. Dyn.* **246**, 779–801 (2017).

100. Labun, K. *et al.* CHOPCHOP v3: expanding the CRISPR web toolbox beyond genome editing. *Nucleic Acids Res.* **47**, W171–W174 (2019).

101. Jao, L. E., Wente, S. R. & Chen, W. Efficient multiplex biallelic zebrafish genome editing using a CRISPR nuclease system. *Proc Natl Acad Sci U S A* **110**, 13904–13909 (2013).

102. Kawakami, K., Shima, A. & Kawakami, N. Identification of a functional transposase of the Tol2 element, an Ac-like element from the Japanese medaka fish, and its transposition in the zebrafish germ lineage. *Proc Natl Acad Sci U S A* **97**, 11403–11408 (2000).

103. Snyder, G. A. *et al.* Functional characterization of Hexacorallia phagocytic cells. *Front. Immunol.* **12**, 662803 (2021).

104. Van Keymeulen, A. *et al.* Epidermal progenitors give rise to Merkel cells during embryonic development and adult homeostasis. *J. Cell Biol.* **187**, 91–100 (2009).

105. Harel, I. *et al.* Distinct origins and genetic programs of head muscle satellite cells. *Dev. Cell* **16**, 822–832 (2009).

106. Gruenbaum-Cohen, Y. *et al.* The actin regulator N-WASp is required for muscle-cell fusion in mice. *Proc. Natl. Acad. Sci.* **109**, 11211–11216 (2012).

107. Nathan, E. *et al.* The contribution of Islet1-expressing splanchnic mesoderm cells to distinct branchiomeric muscles reveals significant heterogeneity in head muscle

development. *Development* **135**, 647–657 (2008).

108. Theis, S. *et al.* The occipital lateral plate mesoderm is a novel source for vertebrate neck musculature. *Development* **137**, 2961–2971 (2010).

109. Harel, I. & Tzahor, E. Head muscle development. in *Craniofacial Muscles* 11–28 (Springer, 2012).

110. Harel, I. *et al.* Pharyngeal mesoderm regulatory network controls cardiac and head muscle morphogenesis. *Proc Natl Acad Sci U S A* **109**, 18839–18844 (2012).

111. Benayoun, B. A. *et al.* Remodeling of epigenome and transcriptome landscapes with aging in mice reveals widespread induction of inflammatory responses. *Genome Res* **29**, 697–709 (2019).

112. Harel, I. & Brunet, A. The African Turquoise Killifish: A Model for Exploring Vertebrate Aging and Diseases in the Fast Lane. *Cold Spring Harb Symp Quant Biol* (2015) doi:10.1101/sqb.2015.80.027524.

113. Hu, L. *et al.* Retaining antigenicity and DNA in the melanin bleaching of melanin-containing tissues. *Int. J. Clin. Exp. Pathol.* **13**, (2020).

114. Turchaninova, M. A. *et al.* High-quality full-length immunoglobulin profiling with unique molecular barcoding. *Nat. Protoc.* **11**, (2016).

115. Andrews, S. FastQC: a quality control tool for high throughput sequence data. 2010. (2017).

116. Krueger, F. Trim galore. *A wrapper tool around Cutadapt FastQC to consistently apply Qual. Adapt. trimming to FastQ files* **516**, 517 (2015).

117. Martin, M. Cutadapt removes adapter sequences from high-throughput sequencing reads. *EMBnet. J.* **17**, 10–12 (2011).

118. Dobin, A. *et al.* STAR: ultrafast universal RNA-seq aligner. *Bioinformatics* **29**, 15–21 (2013).

119. McCarthy, D. J., Chen, Y. & Smyth, G. K. Differential expression analysis of multifactor RNA-Seq experiments with respect to biological variation. *Nucleic Acids Res.* **40**, 4288–4297 (2012).

120. Robinson, M. D., McCarthy, D. J. & Smyth, G. K. edgeR: a Bioconductor package for differential expression analysis of digital gene expression data. *Bioinformatics* **26**, 139–140 (2010).

121. Yu, G., Wang, L.-G., Han, Y. & He, Q.-Y. clusterProfiler: an R package for comparing biological themes among gene clusters. *Omi. a J. Integr. Biol.* **16**, 284–287 (2012).

122. Carlson, M., Falcon, S., Pages, H. & Li, N. org. Hs. eg. db: Genome wide annotation for Human. *R Packag. version* **3**, (2019).

123. Pagès, H., Carlson, M., Falcon, S. & Li, N. AnnotationDbi: Manipulation of SQLite-based annotations in Bioconductor. R package version1. 54.1. (2021).